공학석사학위 논문

Synthesis, Characterization, and Applications of Novel Stable Nitroxide Radical-Bearing π-Conjugated Organic Materials

니트록시드계의 안정한 라디칼을 포함하고 있는
새로운 공액유기분자의 합성, 특성분석,
그리고 응용에 관한 연구

2013 년 8 월

서울대학교 대학원
재료공학부
남 해 림

Synthesis, Characterization, and Applications of Novel Stable Nitroxide Radical-Bearing π-Conjugated Organic Materials

니트록시드계의 안정한 라디칼을 포함하고 있는
새로운 공액유기분자의 합성, 특성분석,
그리고 응용에 관한 연구

지도교수 박 수 영

이 논문을 공학석사 학위논문으로 제출함

2013 년 8 월

서울대학교 대학원

재료공학부

남 해 림

남해림의 석사학위논문을 인준함

2013 년 8 월

위 원 장 _____ (인)

부 위 원 장 _____ (인)

위 원 _____ (인)

Synthesis, Characterization, and Applications of Novel Stable Nitroxide Radical-Bearing π-Conjugated Organic Materials

A THESIS SUBMITTED IN PARTIAL FULFILLMENT OF
THE REQUESTMENTS FOR THE DEGREE OF MASTER
IN ENGINEERING AT THE GRADUATE SCHOOL OF
SEOUL NATIONAL UNIVERSITY

August 2013

BY

Haerim Nam

Supervisor

Soo Young Park

Abstract

Synthesis, Characterization, and Applications of Novel Stable Nitroxide Radical-Bearing π-Conjugated Organic Materials

Haerim Nam
Department of Materials Science and Engineering
The Graduate School
Seoul National University

Attention has been paid to study on nitroxide radicals connected to π-conjugated organic materials due to their unique photophysical, magnetic, and electrochemical properties. Although their potential applications are extensive in biology, chemistry, and physics, insufficient studies on their supramolecular properties in aggregated states limits practical use, so far. Furthermore, only a few examples and strategies have been reported to fabricate nanostructures with nitroxide radicals.

Herein, we report novel π-conjugated organic materials containing nitroxide radicals forming self-assembled nanostructures. The molecules were strategically designed and successfully synthesized in good yield. Unique properties of the nitroxide radicals were investigated by electron spin resonance measurements, UV-Vis spectroscopy, and electrochemical measurements. Interestingly, self-assembled nanoparticles were fabricated via simple re-precipitation methods and exhibited paramagnetism.

Furthermore, as the ascorbic acid sensor applications, the molecules exhibited superior sensing properties with high sensitivity, good selectivity, a broad detection range, and dual-mode detection. Finally, we successfully demonstrated their sensing ability in aqueous conditions by using self-assembled nanoparticles.

Keywords: self-assembly, nanoparticles, nitronyl nitroxide, imino nitroxide, fluorescence sensor, esr sensor, paramagnetism, ascorbic acid

Studnet Number: 2010-20600

Contents

List of Schemes

List of Figures

Chapter 1. Introduction

1.1. Nitroxide Radicals

Stable nitroxide radicals have been widely used in various research fields including physics, chemistry, and biology, due to their unique properties such as paramagnetism, redox-active property and quenching fluorescence of chromophores. These properties come from unpaired electrons, which are generally known to be unstable in common organic materials. The stability of the nitroxide radicals originate from electron delocalization and inhibition of reactions.[1] For example, (2,2,6,6-Tetramethylpiperidin-1-yl)oxyl (TEMPO) radicals have four bulky methyl groups surrounding radicals to hinder the reactivity of the unpaired electron. Another example is nitronyl nitroxide radicals, having unpaired electrons delocalized through two nitrogens and a carbon between nitrogen atoms. These radicals have been reported to be stable more than 6 months even in ambient conditions.[2]

The first unique characteristic of nitroxide radicals is their magnetic properties. In general, organic molecules have diamagnetic property. In contrast, free radicals are paramagnetic due to their own unpaired electrons which are spinning charged body

generating a magnetic field. Any magnetic field can interact with this field, so electron spin resonance measurement can detect the radicals[3]. Especially the *g*-factor obtained by the measurement characterizes the magnetic moment of a particle. Also, each particle has hyperfine structure given by interactions between the unpaired electron and nuclei in the radicals with have non-zero spin like ^{14}N.

The unique photophysical property of nitroxide radicals is that they can quench radiative decay of photo-excited chromophores, if it is covalently or intermolecularly linked to a fluorophore (called FN system). The fluorescence quenching mechanism of FN systems has been explained by the electron exchange-induced intersystem crossing (ISC) and internal conversion (scheme 1.1).[4] Due to connection to the unpaired electron spin, the lowest excited singlet (S_1) state of fluorophore becomes the doublet (D_n) state. After electron exchange interactions with paramagnetic species, molecules become the lowest doublet (D_1) states which had the same multiplicity with the D_n state. Then the second relaxation occurs, and the molecules become the ground doublet states. Therefore, the lifetimes of the excited state is very short compared to those of the transitions from S_1 to S_0. For example, Scheme 1.1 depicts phthalocyanine-nitroxide systems having such a process.

Another important optical aspect of the nitroxide is n-π* absorption bands in visible light region. Aminoxyl oxide has non-bonding orbital of an unpaired electron. The electron can be transited to π* orbital by absorbing photons. Since non-bonding orbital energy level is located between π and π* orbital energy levels, nitroxide radicals

derivatives show colors by absorbing visible light. Also, extinction coefficient of n- π^* transition is small due to less overlapping of both orbitals.

Finally, nitroxides radicals also have reversible electrochemical redox properties. By one-electron reactions, a neutral radical is oxidized to a cation and reduced to an anion. Most of nitroxide radicals have electrochemical reversibility originating from the following two reasons: one is fast electron-transfer rate. When electrochemical reaction occurs, there is no need to break molecular bonds or form new ones, but only electrons are needed to transfer into the open shell electronic structure of the nitroxides.[5] Another is their own molecular structure which can stabilize electrochemically oxidized or reduced ones.

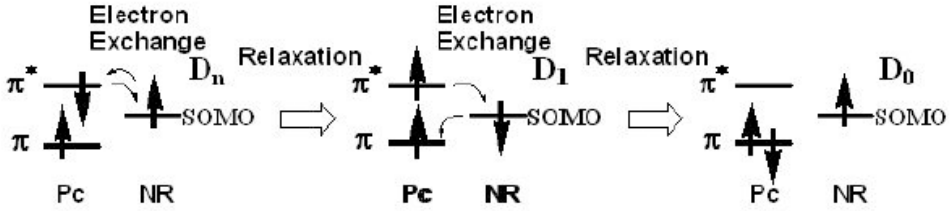

Scheme 1.1. Electron exchange processes in phthalocyanine-nitroxide systems.[4]

1.2. Π-conjugated organic materials linked to nitroxide radicals.

Various applications have been developed exploiting the unique properties of nitroxide radicals. In physics and chemistry, they are utilized as building blocks of ferromagnetic organic materials, [6] spintronic devices, [7] and detectors[8] of radicals generated in chemical reactions. Furthermore, radical organic batteries[5] were realized with reversible electrochemical properties of the nitroxide radicals. Recently, fluorophores bearing nitroxide radicals have been studied for chemical and biological sensors.[9]

Especially, π-conjugated organic materials bearing nitroxide radicals have drawn considerable attentions due to delocalized electrons. The unpaired electron of the nitroxide can significantly affect the electronic structures of π-conjugated organic molecules, leading to innovative properties from a synergetic effect of the unpaired electron and the delocalized electrons.

For example, Sugawara group reported spintronic responses with organic π-conjugated materials containing radical molecules. They reported magetoresistance at below 10 K. Tetrathiafulvalene moieties were used as conducting materials, and electron spins of nitroxide radicals connected to them covalently, guided the conducting electrons. This is the one of the example showing coexistence of conductivity and magnetism.[7]

Furthermore, as building blocks of ferromagnetic materials, after the discovery of bulk ferromagnetism with all organic materials, *p*-nitrophenyl nitronyl nitroxide radical, at 0.60 K, there have been many attempts to rising the temperature showing ferromagnetism. Electron spins of nitronyl nitroxide radicals were reacted to each other, while π-conjugated moiety supported to form ordered crystal structures.[6] Tuning molecular structures for better ordered packing were tried by researchers.

In addition, chromophores linked to nitroxide radicals as antioxidants sensors were reported.[9] Nitroxide radicals turned on and off fluorescence of π-conjugated molecules when they are reacted with reducing agents.

1.3. Self-Assembled Nanostructure and Solid Sate Fluorescence.

Fluorescent organic nanparticles are more variable and flexible in materials synthesis and fabrication of nanoparticles, so it is expected to have superior functions for applications such as biological fluorescent probe, light-emitting diodes, and photovoltaic cells. Organic nanoparticles are usually prepared in self-assembly method. Self-assembly is easy bottm-up approach fabricating nanoparitcles without supports of any complicate equipmetns.

Unfortunately, common organic chromophores often show weak, even no flruorescence in aggregated states, although they exhibit highly luminescent in solution state. This phenamena is called concentration fluorescence quenching. However, the compounds having unique photophysical properties are recently reported. The molecules have enhanced emission in solid state due to J-stacking preventing concentration fluorescence quenching. These kinds of materials also make self-assembled nanoparticles very well with a simple reprecipitation method. For example, one of the materials is CN-TFMBE which has strong intermolecular interactions originated from hydrogen bonding of trifluoromethyl moiety, electrostatic interaction of cyano moiety, and π–π stacking. Due to the structure, it shows bright fluorescence in nanoparticles structures.[13]

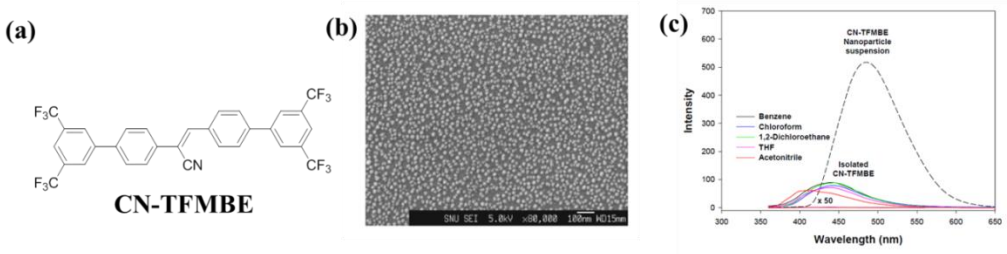

Figure 1.1. Molecular structure (a), nanostructures (b), and emission spectrums (c) of CN-TFMBE.[13]

1.4. Research Objectives

Up to now, π-conjugated oragnic materials with nitroxide radicals have been interested by researchers due to their unique properties. Organic radical materials without π-conjugated backbone have been tried to be fabricated as an organogel[11] and nanoparticles[12] for biological and magnetic applications, so far. However, few studies[10-12] on nanostructured systems of π-conjugated organic materials containing nitroxide radicals have been reported. The materials in nanostructures have great merits such as small-size for bio-applications, inter-spin interactions, and high electrical conductivity. In spite of these advanteges, nanostructures they formed were limited so far to achieve various applications. It is required to develope new strategies of forming their nanostructures.

Herein, we report on the materials design, synthesis, and applications of novel π-conjugated molecules bearing nitroxide radical forming nanoparticles.

We desinged materials containing either nitronyl nitroxide or imino nitroxide which are known to generate dual-funtions, *i.e.* spintronic and optical functions. (Scheme 1.2) For molecular backbone, cyanostilbene and trifluoromethyl moieties were introduced to extend π-conjugation molecules. Due to the strong and unique intermolecular interactions such as hydrogen bonding, electrostatic interaction, and π-π interaction originating from these moieties, the molecules are expected to form self-assembled

nanostructures like nanoparticles without any surfactant, and have no concentration fluorescence quenching. This nanostruture would enhances potentials of various applications.

Characterization was performed mainly from the view of nitronyl nitroxide and imino nitroxide. To investigate the unique properties of nitroxide radicals, electrochemical measurement, electron spin resonance measurement, and UV-Vis spectroscopic measurement were carried out. Furthemore, nanoparticles with novel organic molecules were successfully fabricated, as we intended. The magnetic properties of nanoparticles were also inspected.

Finally, sensing properties were investigated in various systems. The designed materials showed high performance as ascorbic acid sensors in organic solution. It exhibited dual-modal sensing with high sensitivity and good selectivity. We could also successfully detected ascorbic acid by using self-assembled nanoparticles in aqueous suspensions.

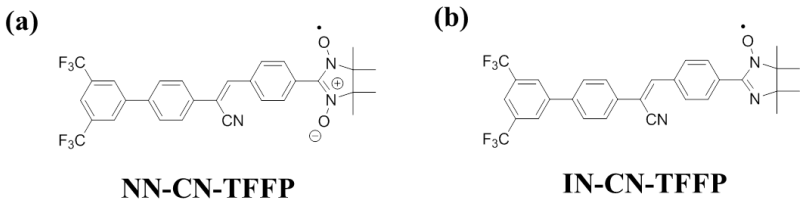

NN-CN-TFFP **IN-CN-TFFP**

Scheme 1.2. Molecular structures of novel organic materials containing nitronyl nitroxide (a) or imino nitroxide (b) radiclas.

1.5. Bibliography

1. A. R. Forrester, R. H. Thomson, *Nature*, **1964**, *203*, 74
2. a) E. F. Ullman, J. H. Osiecki, D. G. B. Boocock , R. Darcy, *J. Am. Chem. Soc.*, **1972**, *94* (20), 7049; b) E. F. Ullman, L. Call, J. H. Osiecki, *J. Org. Chem.*, **1970**, *35* (11), 3623
3. A. R. Forrester, J. M. Hay, R. H. Thomson, *Organic Chemistry of Stable Free Radicals*, *Academic Press London and New York*, **1968**, pp. 7-29
4. a) G. I. Likhtenshtein, S. Nakatsuji, K. Ishii. *Photochem. Photobiol*,. **2007,** *83*, 871; b) G. I. Likhtenshtein *Pure Appl. Chem.*, **2008**, *80* (10), 2125
5. K. Oyaizu, H. Nishide, *Adv. Mater.*, **2009**, *21*, 2339
6. M. Tamura, Y. Nakazawa, D. Shiomi, K. Nozawa, Y. Hosokoshi, M. Ishikawa, M. Takahashi, *Chem. Phys. Lett.*, **1991**, *186* (4), 401
7. a) H. Komatsu, M. M. M, S. Yamamura, Y. Sugawara, K. Suzuki, T. Sugawara *J. AM. CHEM. SOC.*, **2010**, *132*, 4528; b) M. M. Matsushita, H. Kawakami, Y. Kawada, T. Sugawara, *Chem. Lett.,* 2007, 36 (1)
8. a) M. J. Perkins, *Adv. Phys. Org. Chem.*, **1980**, *17*, 1; b) A. L. J. Beckwith, V. W. Bowry and K. U. Ingold, *J. Am. Chem. Soc.*, **1992,** *114*, 4992
9. a) K. Ishii, K Kubo, T. Sakurada, K. Komori, Y. Sakai, *Chem. Commun*., **2011**, *47*, 4932 b) D. Pei, J. Hong, F. Lin, Z. Shi, Z. Chen, H. Nie, X. Guo, *Chem. Commun*., **2011,** *47*, 9492 c) Y. B. Borozdina, V. Kamm, F. Laquai, M.

Baumgarten, *J. Mater. Chem*., **2012**, *22*, 13260

10. Y. Wang, H. Wang, Y. Liu, C. Di, Y. Sun, W. Wu, G. Yu, D. Zhang, D. Zhu, *J. Am. Chem. Soc*., **2006**, 128, 13058
11. Y. Wu, Y. Hirai, Y. Tsunobuchi, H. Tokoro, H. Eimura, M. Yoshio, S. Ohkoshi, T. Kato, *Chem. Sci.*, **2012**, *3*, 3007
12. Y. Nagasaki, *Ther. Deliv.*, **2012**, *3* (2), 165
13. B. An, D. Lee, J. Lee, Y. Park, H. Song, S. Y. Park *J. Am. Chem. Soc*., **2004**, *126* (33), 1023

Chapter 2. Synthesis and Characterization of Novel Radical-Bearing π-Conjugated Organic Materials Forming Paramagnetic Self-Assembled Nanoparticles

2.1. Introduction

Nitroxide radicals have attracted considerable research interests due to their unique properties orginated from unpaired electrons. These unpaired electrons produce various properties such as redox-active property, paramagnetism, and quenching fluorescence of chromophores. Therefore, they have been extensively investigated for various fields of studies such as chemistry, biology, and physics.

Recently, nanostructures of these materials with magnetic properties have been getting attention due to their potential biological applications. Magnetic resonance imaging was realized with organic niroxide radicals linked to dendrimer scaffold using paramagnetic properties[1]. Also, quantum dot (QD)[2] and carbon dot (CD)[3] conjugated nitroxide radicals could detect antioxidants with ESR measurements for future bioapplications.

Herein, we report on synthesis and characteristics of novel nitronyl- and imino-nitroxide derivatives. The two nitroxide molecules were investigated by ESR, UV-Vis spectroscopy, and cyclovoltammetry. In addition, paramagnetic self-assembed nanoparticles, for the first time, were fabricated in an aqueous suspension.

2.2. Experimental

2.2.1. General Information

ESR spectra were recorded in JES-TE 200 and JES-TE 300 (JEOL) at room temperature. The g-factor corrections were obtained using the Mn (g = 1.981, 2.034) as a standard. Spectrometer parameters were microwave power, 1.0 mW; modulation frequency, 100 kHz. Steady state absorbance and fluorescence emission spectra were collected on a UV-1650 PC spectrophotometer (Shimazu) and a Quanta Master 40 (PTI) at room temperature. Relative quantum yield was calculated by using quinine sulfate in 1 N sulfuric acid as fluorescence reference standard (Φ = 0.546). Cyclic voltammetric measurements were performed by using a 273A (Princeton Applied Research) with a one compartment electrolysis cell consisting of a platinum working electrode, a platinum wire counter electrode and a quasi Ag^{+}/Ag electrode as reference. Measurements were proceeded in a 0.5 mM acetonitrile solution with tetrabutylammonium tetrafluoroborate as a supporting electrolyte, at a scan rate of 100 mV/s. All density functional theory (DFT) calculations were carried out in the gas phase using the Gaussian 09 quantum-chemical package.[4] The geometry optimizations for the ground state were performed using B3LYP functional with 6-31G(d,p) basis set. B3LYP corresponds to the combination of Becke's three parameter exchange functional (B3) with a Lee-Yang-Parr fit for the correlation functional (LYP). Vibration frequency calculations at the same level were performed for the obtained structures to

confirm the global minimum. Gauss View 5.0 has been employed for quantum chemical drawing. FE-SEM images of nanoparticles were acquired on a JSM-6330F (JEOL). The samples were obtained by dropping the suspension of nanoparticles solution onto the glass substrates and drying it overnight in ambient conditions. Nanoparticles were prepared by simple precipitation method without surfactants. By this method,[5-6] water was used as a non-solvent for materials in THF solutions. After 70 % - 90 % volume fractions of water addition, materials (2×10^{-5} M) in mixture solution started to aggregate into nano-size particles. Single crystal X-ray diffraction data were collected at 100 K on a Bruker D8 Kappa diffractometer equipped with a SMART APEX II CCD detector with Mo K_α =0.71073 Å) radiation by Dr. Ronald Resel in Graz University of Technology.

2.2.2. Materials

All commercially available reagents were used without further purification unless otherwise stated. Chemicals were purchased from Sigma Aldrich Chemical Co., Tokyo Chemical Industry Co., and Alfa Aeser Co. All syringes, magnetic stirring bars, glassware, and needles were completely dried in a convection oven. Thin layer chromatography (TLC) with commercial TLC plates (silica gel 60 F254, Merck Co.) was used for monitoring reactions. Silica gel column chromatography was performed using silica gel 60 (particle size 0.063-0.200 mm, Merck Co.). ^{1}H and ^{13}C NMR spectra

were measured with a Bruker Avance 300 spectrometer and a Bruker Avance 500 spectrometer, respectively. High resolution mass spectra (HRMS) were acquired by employing JEOL JMS-700 and elemental analyses were performed on a Vario Micro Cube and a CE Flash1112

2.2.3. Synthesis

Target materials were synthesized through the route dipicted in scheme 2.1.

Synthesis of 2,3-Dimethyl-2,3-bis(hydroxylamino)butane (BHA) (1).

Zn dust (10.4 g) and water (20 mL) were added to THF solution (120 mL) containing 2,3-dimethyl-2,3-dinitrobutane (7.04 g, 40.0 mmol) at 0 ^{o}C under Ar atmosphere. Subsequently, an aqueous solution (60 mL) of NH_4Cl (17.2 g, 0.325 mol) was added dropwise with vigorous stirring over 2.5 h. The reaction mixture was stirred for 1.5 h at 0 ^{o}C and then stirred 30 min at room temperature. After reaction, the mixture was filtered and washed with THF. The filtrate was concentrated under reduced pressure and the residue was kept in the refrigerator at -15 ^{o}C for 1 h. The residue was mixed with Na_2CO_3 (20.0 g, 0.189 mol) and NaCl (12.0 g, 0.205 mol) and then carefully charged into a Soxhlet apparatus under Ar atmosphere. The Soxhlet extraction was performed overnight with dichloromethane under Ar atmosphere. The extracted solution was concentrated under vacuum to afford 1.8 g of white powder (Yield =

30 %). ^{1}H NMR (300MHz, DMSO) δ [ppm]: 6.92 (s, 2H, -OH), 5.38 (s, 2H, -NH) 1.00 (s, 12H, -CH_3). HRMS (FAB+, m/z): [M+H]+ calc. for $C_6H_6N_2O_2$, 149.12; found, 149.0.

.

Synthesis of 2-(3',5'-bis(trifluoromethyl)-[1,1'-biphenyl]-4-yl)acetonitrile (2)

2-(4-bromophenyl)acetonitrile (1 g, 5.13 mmol) and (3,5-bis(trifluoromethyl)-phenyl)boronic acid (1.58 g, 6.12 mmol) was dissolved in 50 ml THF. Subsequently, tetrakis (triphenylphosphine) palladium(0) (0.3 g, 0.260 mmol) and aqueous 2 N K_2CO_3 solution (25 ml) was added into the solution sequentially in dark condition. The reaction mixture was stirred and reflux overnight at 80 ^{o}C. The cooled crude mixture was poured into water and titrated to pH 7 with 1.0 M hydrochloric acid. The organic layer extracted by dichloromethane was evaporated in *vacuo*. The product was obtained by column chromatography using ethyl acetate and n-hexane as an eluent. After drying eluent, of 1.29 g of white powder was gained (Yield = 64.1 %). ^{1}H NMR (300 MHz, $CDCl_3$) δ [ppm]: 8.00 (s, 2H, Ar-H), 7.88 (s, 1H, Ar-H) 7.64 (d, 2H, Ar-H, 8.25 Hz), 7.49 (d, 2H, Ar-H, 8.25 Hz), 3.84 (s, 2H, Vinyl-H). ^{13}C NMR (500 MHz, $CDCl_3$) δ [ppm]: 142.3, 138.1, 132.4, 132.2, 130.8, 128.9, 128.0, 127.1, 121.2, 23.3.

Synthesis of (Z)-2-(3',5'-bis(trifluoromethyl)-[1,1'-biphenyl]-4-yl)-3-(4-formylphenyl)acrylon-itrile (3)

Tert-butyl alcohol (30 ml) solution containing 2 (1 g, 3.04 mmol) and

terephthalaldehyde (1.22 g, 9.12 mmol) was stirred at 50 ^{o}C in dark condition. Tetrabutylammonium hydroxide 0.1 M solution in methanol was added dropwise into the solution. The mixture was vigorously stirred for 0.5 h. After reaction, the mixture was poured into methanol with stirring for 1 h and filtered off. Flash column chromatography (ethyl acetate and n-hexane) was performed for purification to afford 0.98 g of green powder (Yield = 73.8 %). ^{1}H NMR (300 MHz, $CDCl_3$) δ [ppm]: 10.10 (s, 1H, -CHO), 8.10 (d, 2H, Ar-H, 8.31 Hz), 8.05 (s, 2H, Ar-H), 8.02 (d, 2H, Ar-H, 8.4 Hz), 7.91 (s, 1H, Ar-H), 7.88 (d, 2H, Ar-H, 8.55 Hz), 7.75 (d, 2H, Ar-H, 8.55 Hz), 7.67 (s, 1H, Vinyl-H). ^{13}C NMR (500 MHz, $CDCl_3$) δ [ppm]: 191.1, 141.9, 140.9, 139.5, 138.9, 137.3, 134.4, 132.5, 132.3, 130.1, 129.8, 128.0, 127.1, 122.2, 121.6, 117.1, 113.9. HRMS (FAB+, m/z): [M+H]+ calc. for $C_{24}H_{13}F_6NO$, 446.09; found, 446.0.

Synthesis of (Z)-2-(3',5'-bis(trifluoromethyl)-[1,1'-biphenyl]-4-yl)-3-(4-(1,3-dihydroxy-4,4,5,5-tetramethylimidazolidin-2-yl)phenyl)acrylonitrile (4)

Methanol (15 ml) and dichloromethane (10 ml) solution of 3 (500 mg, 1.12 mmol) and 1 (500 mg, 3.38 mmol) was stirred overnight under Ar atmosphere at 35 ^{o}C. After the complete reaction, the crude mixture was evaporated under reduced pressure. The product was purified by column chromatography using ethyl acetate and n-hexane. Additionally, the product was washed with n-hexane. After drying solvent, 260 mg of yellow powder was obtained (Yield = 40.2 %). ^{1}H NMR (300 MHz, DMSO) δ [ppm]: 8.42 (s, 2H, Ar-H), 8.21 (s, 1H, Ar-H), 8.14 (s, 1H, Vinyl-H), 8.08 (d, 2H, Ar-H, 8.49

Hz), 7.96 (d, 2H, Ar-H, 4.98Hz), 7.93(d, 2H, Ar-H, 5.25 Hz), 7.86 (s, 2H, -OH), 7.67 (d, 2H, Ar-H, 8.28 Hz), 4.59 (s, 1H, Vinyl-H), 1.10 (d, 12H, Vinyl-H, 10.05 Hz). ^{13}C NMR (500 MHz, $CDCl_3$) δ [ppm]: 145.1, 143.5, 141.6, 137.3, 134.3, 132.8, 131.2, 130.9, 128.9, 128.7, 128.1, 127.3, 126.4, 117.8, 109.0, 89.8, 66.3, 24.3. HRMS (FAB+, m/z): [M+H]+ calc. for $C_{30}H_{27}F_6N_3O_2$, 576.20; found, 576.0.

Synthesis of (Z)-2-(3',5'-bis(trifluoromethyl)-[1,1'-biphenyl]-4-yl)-3-(4-(1-Oxyl-3-oxo-4,4,5,5-tetramethylimidazolidin-2-yl)phenyl)acrylonitrile (5)

The solution of 4 (100 mg, 0.17 mmol) in dichloromethane was vigorously stirred at room temperature. Tetrapropylammonium perruthenate (3.05 mg, 0.0087 mmol) and 4-methylmorpholine N-oxide (20.35 mg, 0.17 mmol) was added to the solution, sequentially. After 1.5 h reaction, the complete reaction was confirmed by TLC. The column chromatography using ethyl acetate and n-hexane was performed for purification to afford 50.63 mg of green powder (Yield = 50.9 %). HRMS (FAB+, m/z): [M+H]+ calc. for $C_{30}H_{24}F_6N_3O_2$, 573.18; found, 573.2. Elemental analysis: calcd. for $C_{30}H_{24}F_6N_3O_2$ C 62.94, H 4.23, N 7.34; found: C 62.70, H 4.30, N 7.12.

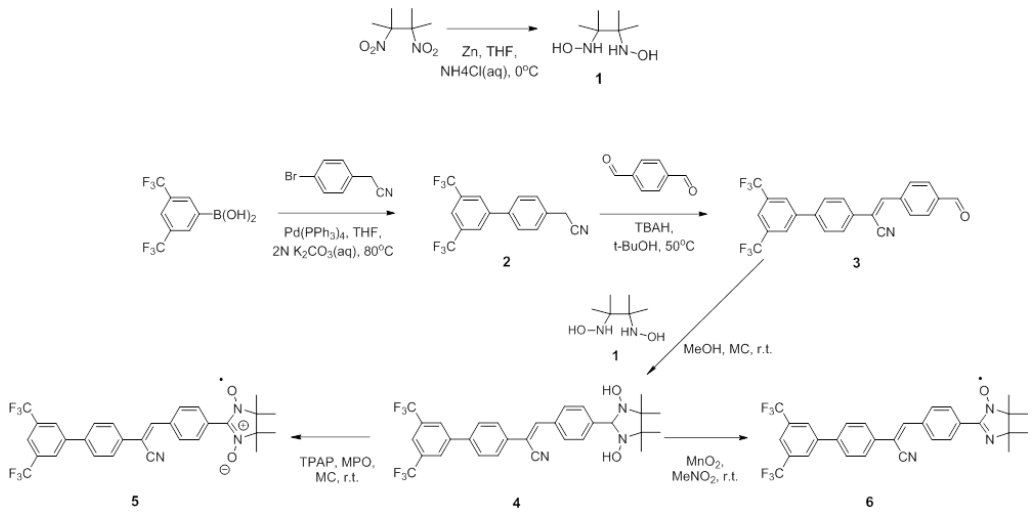

Scheme 2.1. Synthetic route of target materials.

Synthesis of (Z)-2-(3',5'-bis(trifluoromethyl)-[1,1'-biphenyl]-4-yl)-3-(4-(1-Oxyl-4,4,5,5-tetrame-thylimidazolidin-2-yl)phenyl)acrylonitrile (6)

The reaction mixture of 4 (100 mg, 0.17 mmol) and MnO_2 (226 mg, 2.60 mmol) in $MeNO_2$ was stirred overnight and filtered. After dilution of the solution with n-heptane (6 mL), the mixture was concentrated under reduced pressure. The product was purified by column chromatography with ethyl acetate and n-hexane to afford 60 mg of orange powder (Yield = 62.0 %). Elemental analysis: calcd. for $C_{30}H_{24}F_6N_3O$: C 64.75, H 4.35, N 7.55; found: C 64.61, H 4.39, N 7.44.

2.3. Results and Discussions

2.3.1. ESR Spectrum

The molecules containing nitronyl nitroxide radical **5** and imino nitroxide radical **6** exhibited ESR spectrum in benzene solution (10^{-3} M) at room temperature, respectively. The nitrogen atom having spin I = 1, interacts with an unpaired electron to split the electron resonance line of a molecule into three equally intense lines.[7] Due to two equivalent nitrogen nuclei of the imidazolyl moiety in NN-CN-TFFP, five lines were obtained with an intensity ratio, 1 : 2 : 3 : 2 : 1 as shown in Figure 2.1a.[8] The spectrum shows g value, g = 2.0075, and coupling constant, $|a_N|$ = 0.764 mT, which were the typical value of nitronyl nitroxide radical.[9]

On the other hand, non equivalent nitrogen nuclei of IN-CN-TFFP induced seven line patterns with an intensity ratio 1 : 1 : 2 : 1 : 2 : 1 : 1 as shown in Figure 2.1b. It had g = 2.0069, $|a_{N1}|$ = 0.889 mT, $|a_{N2}|$ = 0.467 mT which were consistent with the value of other imino nitroxides reported.[10]

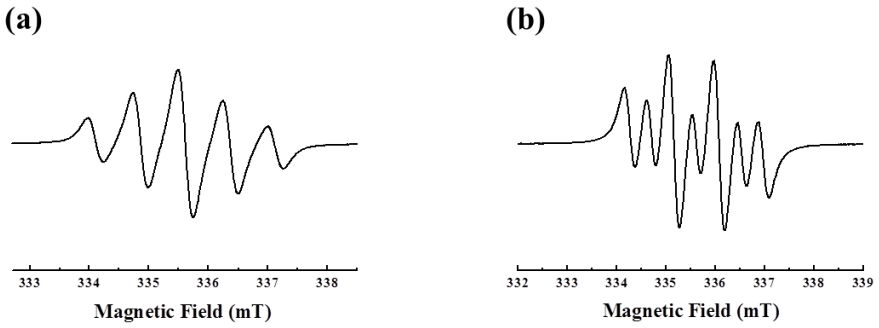

Figure 2.1. ESR spectra of NN-CN-TFFP (a) and IN-CN-TFFP (b).

2.3.2. Photophysical Property

Figure 2.2 depicts the UV-Vis absorption spectra of the molecules **5** and **6** were measured in ethyl acetate solution (3×10^{-5} M). Two dominant bands were obtained in both molecules, respectively. The first set of bands was lying at 358 nm and 337 nm wavelength, respectively, with very high absorption coefficient around 50000 M^{-1} cm^{-1}. The signals correspond to π- π^* transition of aromatic backbone. Due to longer conjugation of nitronyl nitroxide than that of imino nitroxide, the absorption maxima of nitronyl nitroxide was located at longer wavelength.

The second set of absorption bands exhibited very low molar absorptivity at 530 nm and 460 nm, respectively. Therefore, colors of solutions were blue-green and orange-red, respectively. These bands correspond to the n-π^* transitions of the aminoxyl oxide moieties.[11] These bands are also good criteria to distinguish different nitroxide species (i.e. nitronyl *vs* imino radicals.). This phenomena is also confirmed by DFT calculations. As shown in Figure 2.3, singly occupied molecular orbital (SOMO), non-bonding orbital, have very small space overlapping with lowest unoccupied molecular orbital (LUMO), π^* orbital. It explained the small extinction coefficient of n-p* transitions.Furthermore, the gap between energy levels of LUMO and SOMO of IN-CN-TFFP is bigger than that of NN-CN-TFFP consistent with their absorption spectra in longer wavelengths.

Luminescence of the nitroxide molecules was hard to detect due to their very low quntum yield, which can be explained by the ISC theory mentioned in the Chapter 1. From the DFT results, it was found that SOMO energy levels are located in between highest occupied molecular orbital (HOMO) and LUMO energy levels, resulting in sufficient energy matching for electron exchange relaxation. Novel stable nitroxide radicals materials (NN-CN-TFFP and IN-CN-TFFP) showed paramagnetism, redox-active property and quenched fluorescent property in the previous chapter. By combining these properties, the materials are capable to detect ascorbic acid (AA) bimodally, fluorescence and magnetism, which is a very important nutrient for biological functions.[1] The materials are also expected to detect ascorbic acid in aqueous systems by using their self-assembled paramagnetic nanoparticles.

As the conventional dual-mode ascorbic acid sensors, nitroxide radicals linked to luminophores were reported mainly using TEMPO radicals.[3-4] These materials reported exhibited low sensitivity and poor selectivity. However, nitronyl nitroxide and imino nitroxide derivatives high sensitivity and better selectivity.[5] Nevertheless, it has a few examples.

FN systems for detecting ascorbic acid were also studied in aqueous environment because ascorbic acid is water-soluble materials. Three strategies were considered for using these derivatives in water systems. Firstly, water-soluble polymers were selected as fluorophores and connected to nitroxide radicals[3b)]. Secondly, hydrophobic fluorescent probes were covered with liposomes to load it into water systems[3a)]. Lastly,

surface engineering of quantum dots and carbon dots were introduced[5].

Herein, we report application potential of the previously synthesized π-conjugated nitroxide molecules (NN-CN-TFFP and IN-CN-TFFP) as ascorbic acid with high sensitivity, dual-mode detection ability, high selectivity, and broad detection ranges. Their self-assembled nanoparticles could also take roles as ascorbic acid dual-mode probes even in aqueous solution.

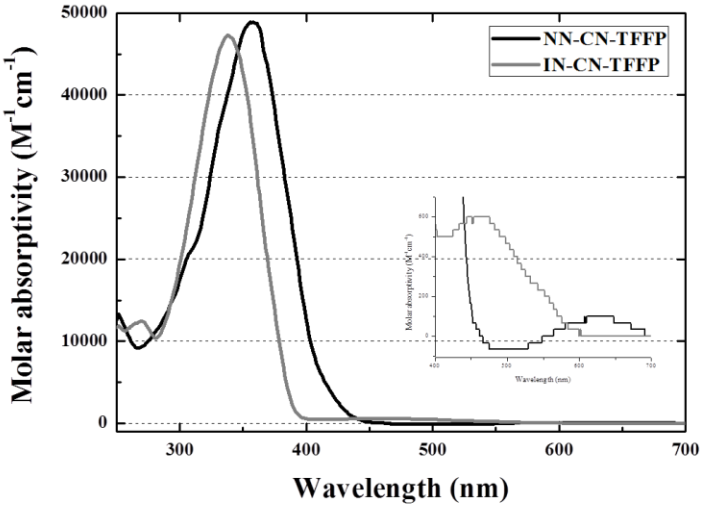

Figure 2.2. UV-Visible absorption spectra of NN-CN-TFFP (black line) and IN-CN-TFFP (grey line) in EA solution ($c = 3 \times 10^{-5}$ mol L^{-1}).

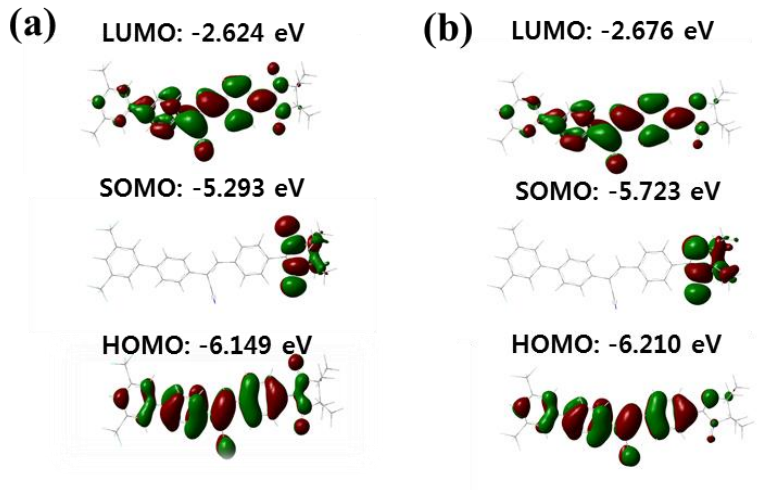

Figure 2.3. Molecular orbitals and their energy levels of NN-CN-TFFP (a) and IN-CN-TFFP.

2.3.3. Electrochemical Property

NN-CN-TFFP exhibited a reversible redox wave at 0.39 V *versus* Ag/Ag+. (Figure 2.3 a) This wave well corresponded with nitronyl nitroxide radical/oxoammonium cation couple (Scheme 2.2 (a)).[12] Because of resonance structure and steric hindrance of oxoammonium cation, it shows reversible characteristics[12]. Compared with a redox potential of ferrocene (0.03 V *vs* Ag/Ag+), SOMO energy level of NN-CN-TFFP was acquired as - 5.16 eV. On the other hand, quasi-reversible redox of molecules occurred at - 1.10 V *vs* Ag/Ag+, which corresponds to reduction of nitronyl nitroxide radical to aminoxyl anion. Quasi-reversibility proved the stabilities of each chemical species.

IN-CN-TFFP also displayed the similar electrochemical behavior with NN-CN-TFFP (Figure 2.3 b). In contrast, only a quasi-reversible redox wave, however, was observed at 0.84 V vs Ag/Ag+. SOMO energy level was calculated to be -5.61 eV. The difference between SOMO energy levels of NN-CN-TFFP and IN-CN-TFFP are 0.45 eV and well consistent with the DFT results (0.43 eV). The poor reversibility of oxidized species of IN-CN-TFFP is attributed to that the oxoammonium cation of IN-CN-TFFP has shorter conjugation length than that of NN-CN-TFFP.

The redox waves of the molecules did not change at all even after 5 redox cycles. It means that any significant further reactions or decompositions did not occur.

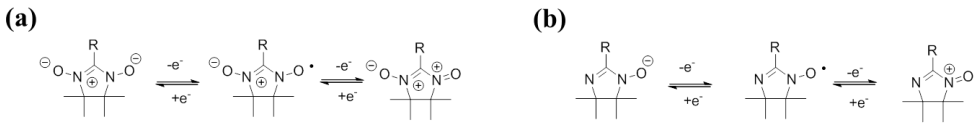

Scheme 2.2. Redox mechanism of NN-CN-TFFP (a) and IN-CN-TFFP (b).

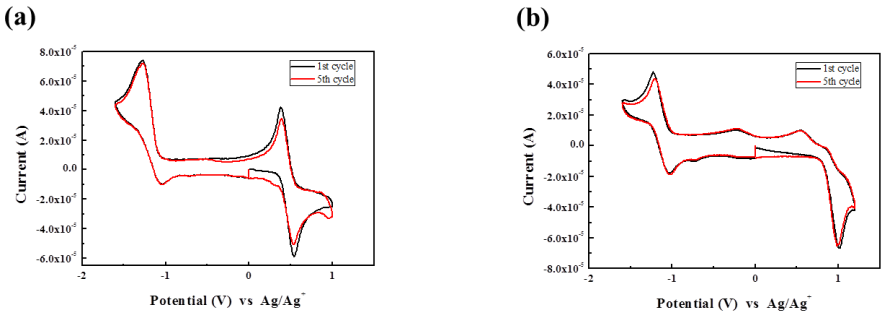

Figure 2.4. Cyclic voltammogram of a solution of 3.0 mM NN-CN-TFFP (a) and IN-CN-TFFP in acetonitrile containing 0.1 M $TBAPF_6$ at a sweep rate of 0.1 Vs^{-1} and using a glassy carbon electrode.

2.3.4. Paramagnetic Self-Assembled Nanoparticles.

As the molecular design strategy we devised, the molecules formed self-assembled nanostructure. The nanoparticles were prepared by simple reprecipitation method without surfactants. By this method,[5-6] water was used as a non-solvent for molecules in THF solution (2×10^{-5} mol L^{-1}). Nano-size particles aggregated after 70 % ~ 90 % volume fraction of water addition. Field-emission scanning electron microscopy (FE-SEM) images show well-formed nanoparticles. (Figure 2.5) The larger water fraction of the mixtures, it shows the larger size of particles, from sub-100 nm to sub-1 μm.

All NN-CN-TFFP nanoparticles showed paramagnetic characteristics, as we expected. To the best of our knowledge, this is the first example of self-assembled paramagnetic nanoparticles using organic nitroxides small molecules. The interesting feature is that the peak of ESR spectrum becomes broader when nanoparticles were formed in 80 and 90 vol% water/THF solutions than in 70 vol%. (Figure 2.7). This is because additional intermolecular hyperfine splitting occurred by nitrogen atoms of neighboring molecules in the nanoparticles. Since size of particles increased as water portion increased, nitroxide radicals might interacted with more neighboring molecules in larger particles to exhibit broader ESR peak.

Single crystal analysis of NN-CN-TFFP is performed for elucidating the inter-spin interactions in the nanoparticles. It has been reported that spin-spin interaction occurs when the distance is below 4 Å. Unfortunately, NN-CN-TFFP exhibited dimer-like

stacking (Figure 2.9a) and the intermolecular distance between nitroxide radicals are 7.69 Å through the columnar direction. The shortest distance between radicals through intercolumnar direction is 5.44 Å, which are shown in Figure 2.9 (b). As a result, each spin is expected to have independent interaction with applied magnetic field without any kind of inter-spin interactions such as ferro- or anti-ferromagnetic interactions.

IN-CN-TFFP nanoparticles show the similar nanoparticle formation with NN-CN-TFFP. Different from NN-CN-TFFP, all nanoparticles prepared exhibited one broaden ESR peak.

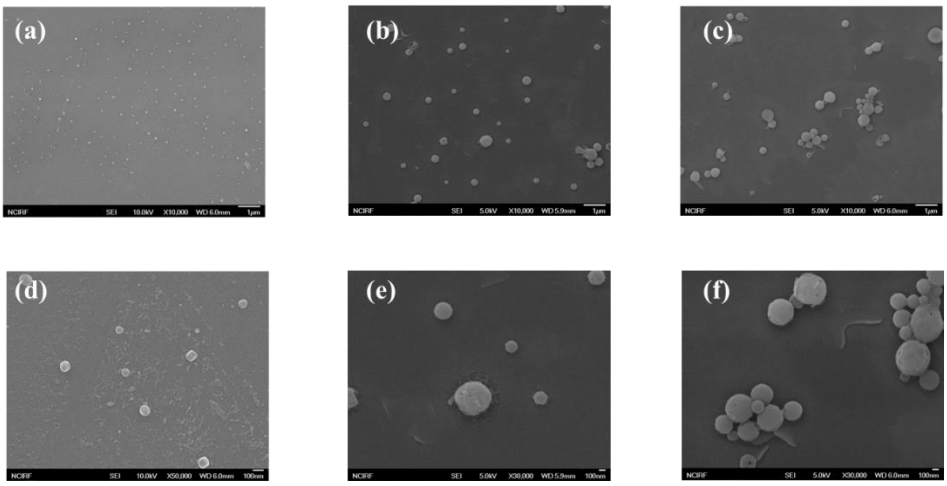

Figure 2.5. FE-SEM images of NN-CN-TFFP in 70 vol% (a), 80 vol% (b), and 90 vol% (c) water/THF solutions. And magnified images are below in 70 vol% (d), 80 vol% (e), and 90 vol% (f) water/THF solutions.

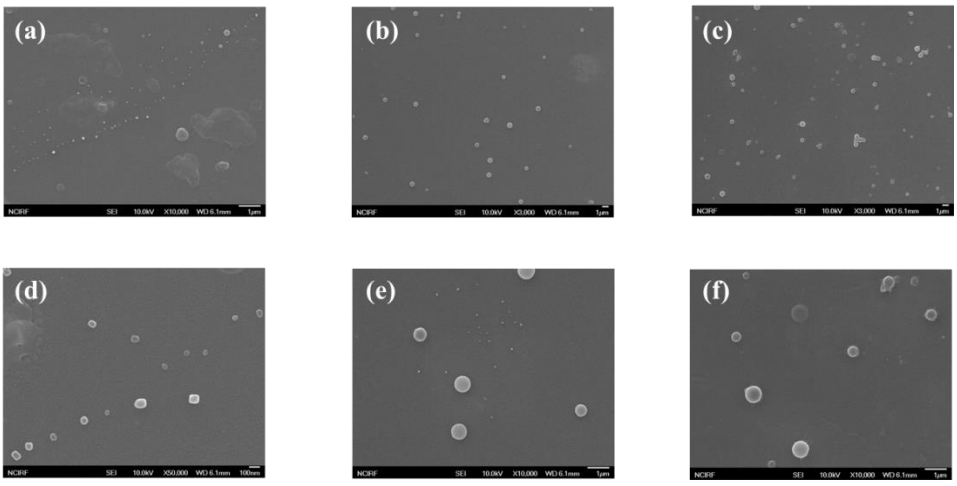

Figure 2.6. FE-SEM images of IN-CN-TFFP in 70 vol% (a), 80 vol% (b), and 90 vol% (c) water/THF solutions. And magnified images are below in 70 vol% (d), 80 vol% (e), and 90 vol% (f) water/THF solutions.

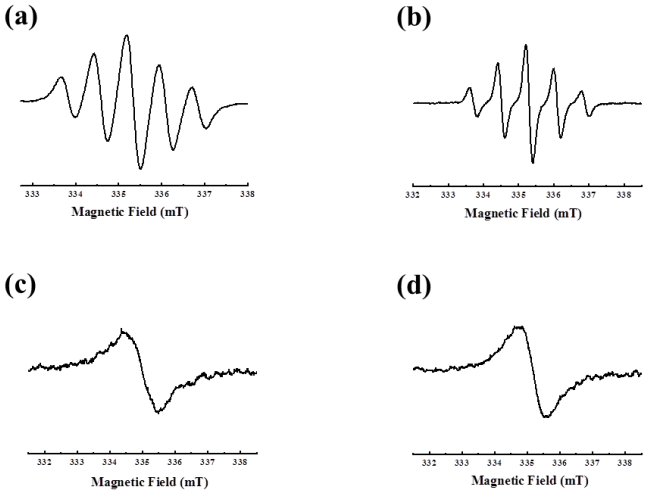

Figure 2.7. ESR spectrums of NN-CN-TFFP in THF solution (a), 70 vol% (b), 80 vol% (c), and 90 vol% (d) water/THF solutions.

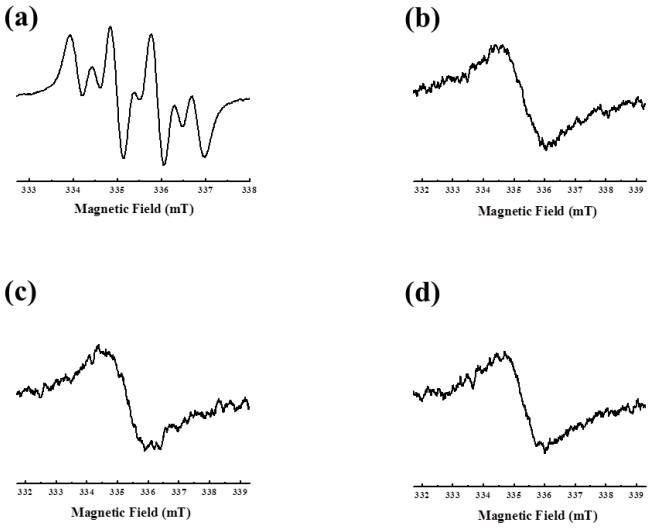

Figure 2.8. ESR spectrums of IN-CN-TFFP in THF solution (a), 70 vol% (b), 80 vol% (c), and 90 vol% (d) water/THF solutions.

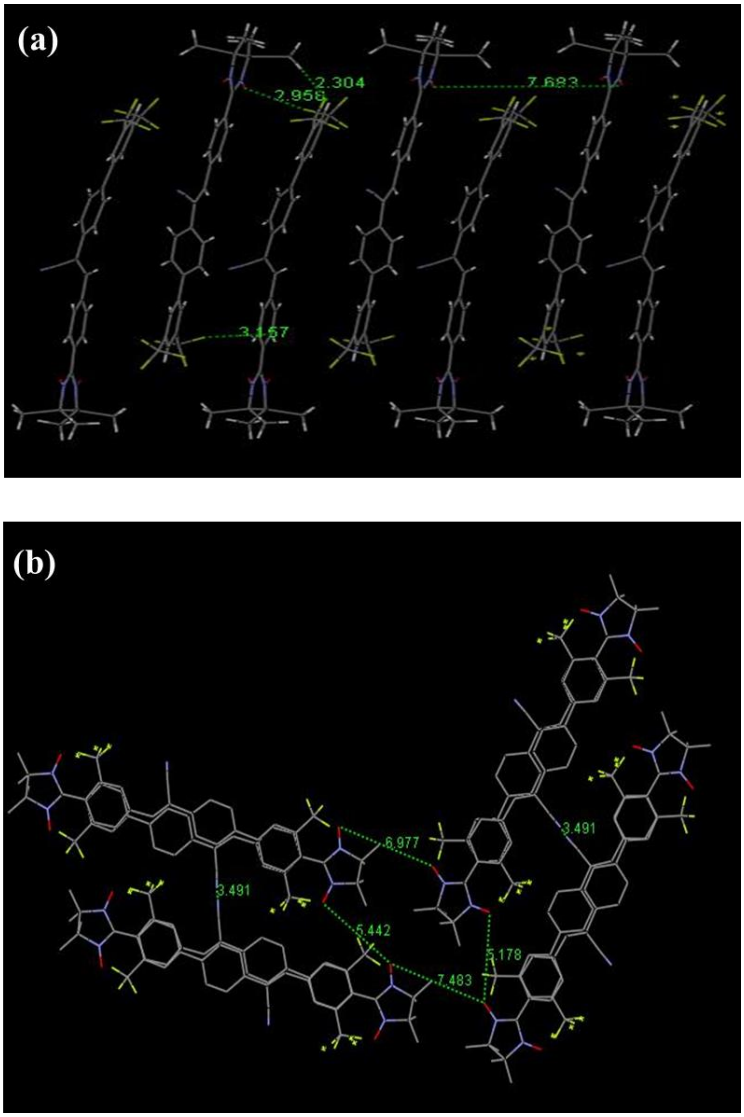

Figure 2.9. Single crystal analysis of NN-CN-TFFP.

2.4. Conclusion

We designed and successfully synthesized novel organic π-conjugated molecules bearing nitroxide radicals. Two different molecules containing nitronyl nitroxide and imino nitroxide exhibited typical 5 lines and 7 lines patterned ESR signals, respectively. The fingerprints of these radicals were shown in absorption bands in the range of 400 nm - 800 nm wavelengths shown in absorption spectrum. Also, unpaired electrons make the molecules have reversible redox-active properties. Furthermore, characterized molecules were fabricated to self-assembled paramagnetic nanoparticles successfully. Nanostructured materials showed broadened ESR signals clearly. In this work, we firstly fabricated paramagnetic self-assembled nanoparticles using all organic small molecules without any additional surfactants by the simple reprecipitation method. The realization of magneto-nanoparticles would lead advanced study of biological systems requiring magnetic materials.

2.5. Bibliography

1. A. Rajca, Y. Wang, M. Boska, J. T. Paletta, A. Olankitwanit, M. A. Swanson, D. G. Mitchell, S. S. Eaton, G.h R. Eaton, S. Rajca, *J. Am. Chem. Soc.*, **2012**, *134*, 15724
2. W. Chen, X. Wang, X. Tu, D. Pei, Y. Zhao, X. Guo, *Small*, **2008**, *4*(6), 759
3. F. Lin, D. Pei, W. He, Z. Huang, Y. Huang and X. Guo, *J. Mater. Chem.*, **2012**, *22*, 11801
4. Gaussian 09, Revision A.02, M. J. Frisch, G. W. Trucks, H. B. Schlegel, G. E. Scuseria, M. A. Robb, J. R. Cheeseman, G. Scalmani, V. Barone, B. Mennucci, G. A. Petersson, H. Nakatsuji, M. Caricato, X. Li, H. P. Hratchian, A. F. Izmaylov, J. Bloino, G. Zheng, J. L. Sonnenberg, M. Hada, M. Ehara, K. Toyota, R. Fukuda, J. Hasegawa, M. Ishida, T. Nakajima, Y. Honda, O. Kitao, H. Nakai, T. Vreven, J. A. Montgomery, Jr., J. E. Peralta, F. Ogliaro, M. Bearpark, J. J. Heyd, E. Brothers, K. N. Kudin, V. N. Staroverov, R. Kobayashi, J. Normand, K. Raghavachari, A. Rendell, J. C. Burant, S. S. Iyengar, J. Tomasi, M. Cossi, N. Rega, J. M. Millam, M. Klene, J. E. Knox, J. B. Cross, V. Bakken, C. Adamo, J. Jaramillo, R. Gomperts, R. E. Stratmann, O. Yazyev, A. J. Austin, R. Cammi, C. Pomelli, J. W. Ochterski, R. L. Martin, K. Morokuma, V. G. Zakrzewski, G. A. Voth, P. Salvador, J. J. Dannenberg, S. Dapprich, A. D. Daniels, Ö. Farkas, J. B. Foresman, J. V. Ortiz, J. Cioslowski, and D. J. Fox, Gaussian 09, revision A.02; Gaussian,

Inc., Wallingford CT, 2009

5. a) H. Kasai, H. S. Nalwa, S. Okada, H. Oikawa, H. Nakanish, *Handbook of Nanostructured Materials and Nanotechnology*, Academic press, **2000** b) D. Horn, J. Rieger, *Angew. Chem. Int. Ed*., **2001**, *40*, 4330
6. B. An, S. Kwon, S. Jung, S. Y. Park, *J. Am. Chem. Soc.*, **2002**, *124*, 14410
7. A. R. Forrester, J. M. Hay, R. H. Thomson, *Organic Chemistry of Stable Free Radicals*, *Academic Press London and New York*, **1968**, pp. 7-29
8. J. E. Wertz and J. R. Bolton, *Electron Spin Resonance*, *Elementary Theory and Practical Applications*, VCH, New York, **1986**
9. E. F. Ullman, J. H. Osiecki, D. G. B. Boocock and R. Darcy, *J. Am. Chem. Soc.*, **1972**, *94*, 7049
10. Y. B. Borozdina, V. Kamm, F. Laquai, M. Baumgarten, *J. Mater. Chem*., **2012**, *22*, 13260
11. E. F. Ullman, L. Call and J. H. Osiecki, *J. Org. Chem.*, 1970, **35**, 3623
12. J. Lee, E. Lee, S. Kim, G. S. Bang, D. A. Shultz, R. D. Schmidt, M. D. E. Forbes, H. Lee, *Angew. Chem. Int. Ed.*, **2011**, *50*, 4414

Chapter 3. Novel Radical-Bearing π-Conjugated Organic Materials for Dual-Modal Ascorbic Acid Sensors

3.1. Introduction

Novel stable nitroxide radicals materials (NN-CN-TFFP and IN-CN-TFFP) showed paramagnetism, redox-active property and quenched fluorescent property in the previous chapter. By combining these properties, the materials are capable to detect ascorbic acid (AA) bimodally, using fluorescence and magnetism, which is a very important nutrient for biological functions.[1] The materials are also expected to detect ascorbic acid in aqueous systems by using their self-assembled paramagnetic nanoparticles.

As the conventional dual-mode ascorbic acid sensors, nitroxide radicals linked to luminophores were reported mainly using TEMPO radicals.[2,3] These materials exhibited low sensitivity and poor selectivity. However, it has been reported that nitronyl nitroxide and imino nitroxide derivatives higher sensitivity and better

selectivity.[4] Nevertheless, it has a few examples.

On the other hand, FN systems for detecting ascorbic acid were studied in aqueous environment because ascorbic acid is water-soluble materials. Three strategies were considered for using these derivatives in water systems. Firstly, water-soluble polymers were selected as fluorophores and connected to nitroxide radicals[2b)]. Secondly, hydrophobic fluorescent probes were covered with liposomes to load it into water systems[2a)]. Lastly, surface engineering of quantum dots and carbon dots were introduced.[3]

Herein, we report application potential of the previously synthesized π-conjugated nitroxide molecules (NN-CN-TFFP and IN-CN-TFFP) as ascorbic acid sensors with high sensitivity, dual-mode detection ability, high selectivity, and broad detection ranges. Their self-assembled nanoparticles could also take roles as ascorbic acid dual-mode probes even in aqueous solution.

3.2. Experimental

3.2.1. General Information

Transmission electron microscophy (TEM) images were obtained with TEM-CM30 (Philips) at Korea Institute of Science and Technology (KIST). Samples were prepared by dropping the nanoparticles suspension on the grid and drying it.

3.2.2. Materials

2-(4-Hydroxyphenyl)ethanol (tyrosol (Tyr), 98%, Sigma Aldrich Co.), hydroquinone (HQ, 99%, Sigma Aldrich Co.), L-cysteine (Cys, 97%, Sigma Aldrich Co.), L-ascorbic acid (AA, Sigma Aldrich Co.), L-glutathione reduced (GSH, Sigma Aldrich Co.), and butylatedhydroxytoluene (BHT, analytical standard, Sigma Aldrich Co.) were purchased commercially and used without further purification.

3.2.3. Titration Procedure

For titration in the organic solution, up to 0.03 mL of analytes stock solution (2×10^{-1}, 2×10^{-2}, 2×10^{-3} M) was added to 3.0 mL of 2×10^{-5} M solution of NN-CN-TFFP and IN-CN-TFFP in methanol. Analytes were dissolved in methanol (ascorbic acid,

butylated hydroxy toluene) and distilled water (glutathione, hydroquinone, tyrosol). After addition of stock solution, the solution was shaked for 3 min to reach equilibrium. Subsequently, UV-Vis absorption, fluorescence, and ESR spectra were obtained.

In nanoparticles states, similar procedure taken with titration in the organic solution. In contrast, ascorbic acid was dissolved in distilled water. Also, mechanical vortexer was used to reach equilibrium of the sensing reaction.

3.3. Results and Discussion

3.3.1. Sensor Properties in Organic Solutions

3.3.1.1. Sensitivities and Quenching Mechanisms

The sensor properties of novel organic materials (NN-CN-TFFP and IN-CN-TFFP) were examined thoroughly. In methanol solution (2 x 10^{-5} M), the molecules exhibited high-performance sensor properties.

First of all, it shows a dual-modal detection property. One mode is ESR signals in magnetic field, and another is photoluminescence. Nitroxide radicals quenched the fluorescence of chromophores through the electron exchange interaction mechanism. When AA reacted with the nitroxide radicals as an antioxidant, it reduces the nitroxide radical and hence generates a diamagnetic hydroxylamine, leading to ESR intensity decrease. Although all radicals disappear, the fluorescence of the molecules was turned on only slightly because additional deactivation pathway still exists. Lone pair electrons of imidazole units of nitronyl nitroxide is known to quench radiative decay of excited state electron through photoinduced electron transfer (PET). This additional pathway quenches the fluorescence of the backbone more efficiently than other nitroxides, resulting in high on-off contrast ratio. The quenching site can be arrested by protonation process with acid molecules. Ascorbic acid has sufficient acidity to protonate NN-CN-TFFP and IN-CN-TFFP and recovers their fluorescence completely.

These sequential reactions are found in a spectroscopic titration result. UV-Vis absorption intensity change is examined with addition of AA. The isosbestic points at 325 nm and 380 nm were observed when the presence of less than 16 μM AA concentration (Figure 3.4 (a)). Further increase of AA concentration generated new trend of the absorption spectra change (Figure 3.4 (C)). Each range was consistent with the ESR detection region and the fluorescence detection region. Therefore, it is plausible that the two reactions, redox reaction and protonation were taking place sequentially. Proposed reaction mechanisms are shown in Scheme 3.1.

Secondly, the sensors displayed high on-off ratio of PL intensity (maximum fluorescence recovery efficiency F/Fo = ~ 250) which were not shown in TEMPO radical derivatives[3]. The phenomena could be explained by the structures of the radicals. Different from TEMPO radicals connected to a fluorophore with σ bond, radicals linked to a backbone through π-conjugations enhance the interaction between a quencher and a chromophore. SOMO calculated by DFT method overlaps with HOMO and LUMO of backbone. Also, not only nitroxide radicals quenched backbones with intersystem crossing mechanism, but also imidazole moiety additionally lead non-radiative decay by photoinduced electron transfer mechanism.

Lastly, it is interesting that sensors cover very extensive detection range. Figure 3.1 and 3.2 illustrates ESR and fluorescence spectra change of NN-CN-TFFP and IN-CN-TFFP in the presence of various concentration of AA. When AA concentration

increases, their fluorescence intensity increases while their ESR signal decreases. The linear decrease of ESR double integration value was observed in the range of 0 ~ 12 x 10^{-6} M and 0 ~ 14 x 10^{-6} M AA concentration with limit of detection (LOD), 9.4 x 10^{-7} M and 6.80 x 10^{-7} M for NN-CN-TFFP and IN-CN-TFFP, respectively.[5] Significant fluorescence turn-on was observed after ESR signal completely disappeared (Figure 3.4 and 3.6). Although linear increase region of *F/Fo* is only from 1 x 10^{-5} M to 2 x 10^{-4} M of AA concentrations, we could also plot the *F/Fo* fitting curve linearly with respect to logarithm of AA concentration range from 1x10^{-4} M to 2x10^{-3} M. These correlation factors and fitting curves are displayed in Figure 3.1 and 3.2.

Not only the dual modes contribute detection range complementarily, but also binding constants and sensitivity effect on broad detection range. To investigate equilibrium constants (K) of two sequential reactions, Benesi-Hildebrand equation ($\Delta A/b = (Q_t K \Delta\varepsilon[L])/(1 + K[L])$) was used.[9] The reciprocal of UV-Vis absorbance change (ΔA) at a specific wavelength (λ_{ab}) was plotted with respect to reciprocal of ascorbic acid molar concentration ([L]). The equation for the 1:1 complex formation is well matched to the experimental results with both reaction ranges: redox reaction and protonation. The calculated binding constant of redox reaction (K_1) was 2.14 x 10^5 M^{-1} and 7.60 x 10^4 M^{-1} (calculated at λ_{ab} = 351 and 336 nm), while one of protonation (K_2) was 1.99 x 10^3 M^{-1} and 1.12 x 10^3 M^{-1} (calculated at λ_{ab} = 395 and 400 nm) for NN-CN-TFFP and IN-CN-TFFP, respectively. With 2x10^{-4} M of AA concentration, the molecules showed

250- and 150-fold increase in fluorescence for NN-CN-TFFP and IN-CN-TFFP, respectively. . The high sensitivity with dual binding modes results in a broad detection range.

This property makes the materials superior to quantify AA over all useful concentration ranges with a single probe. The useful AA concentration in human blood plasma or serum is from 10 μM to 100 μM for clinical applications[6] while food contains 0.1 to 3 mM[7]. Also, pharmaceutical approach needs 0.3 to 20 mM of AA concentration.[8]

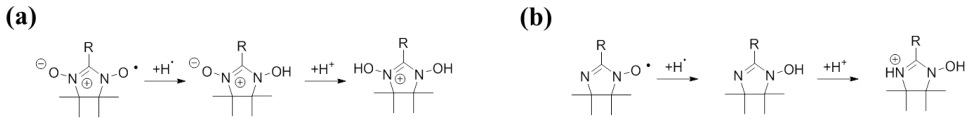

Scheme 3.1. Proposed reaction with NN-CN-TFFP (a) and IN-CN-TFFP (b).

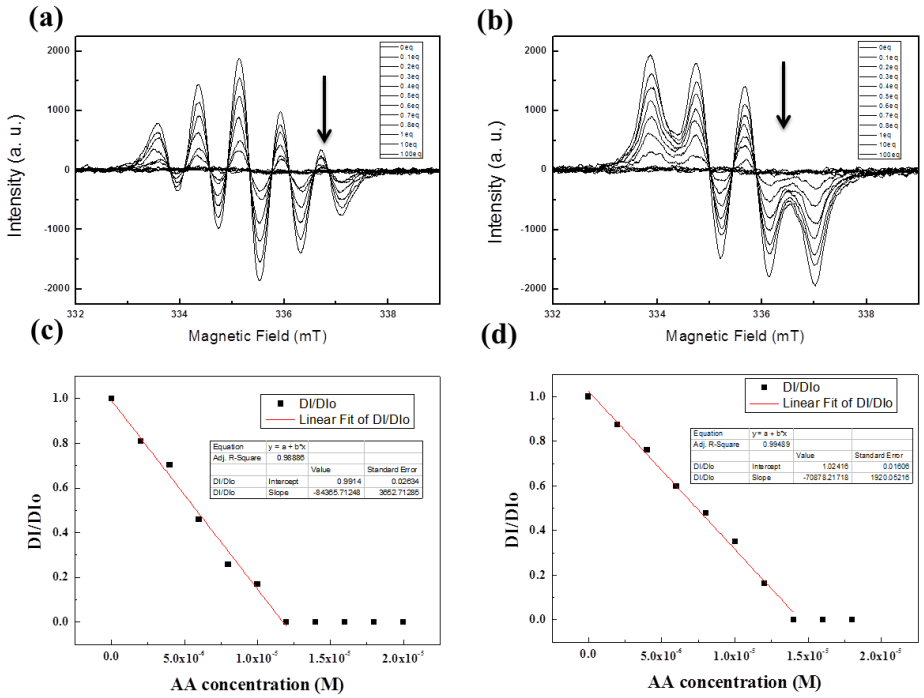

Figure 3.1. ESR spectrum change of NN-CN-TFFP (a) and IN-CN-TFFP (b) in MeOH (2 x 10^{-5} M) with injection of ascorbic acid from 0.1 eq. to 1eq. ESR signals change (DI(Double Integration)/DIo([AA] = 0)) in the respect to ascorbic acid concentration was depicted in (c) and (d) for NN-CN-TFFP and IN-CN-TFFP, respectively. Correlation curves and factors were described in the graphs.

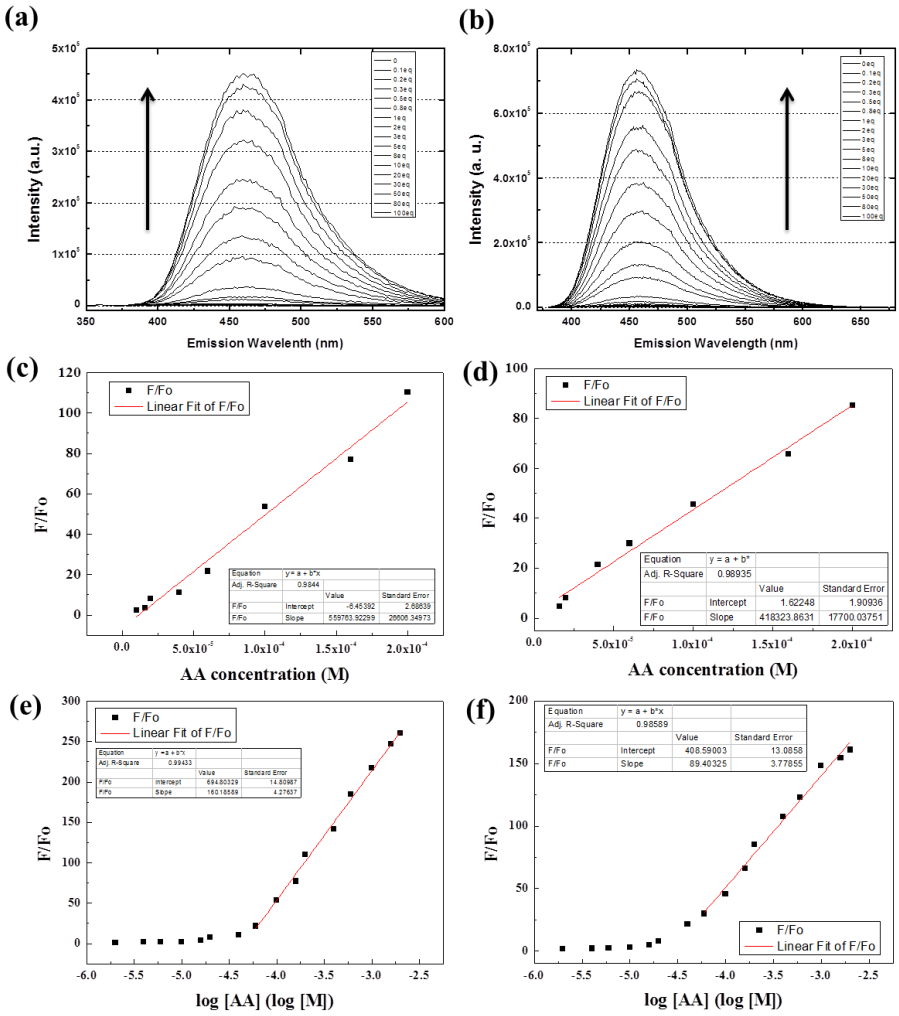

Figure 3.2. PL spectrum change of NN-CN-TFFP (a) (λ_{ex} = 326 nm) and IN-CN-TFFP (b) (λ_{ex} = 362 nm) in MeOH solution (2 x 10^{-5} M) with injection of ascorbic acid from 0.1 eq. to 100 eq. *F/Fo* change in the respect to ascorbic acid concentration was depicted in (c), (e) and (d), (f) for NN-CN-TFFP and IN-CN-TFFP, respectively. (c), (d) described. Correlation curves and factors were described in the graphs.

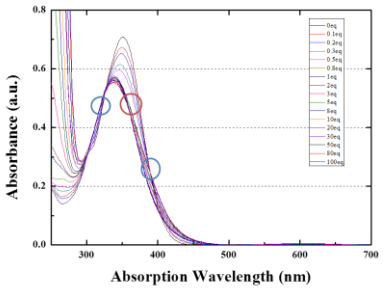

Figure 3.3. Absorption spectrum change of NN-CN-TFFP in MeOH solution (2 x 10^{-5} M) with injection of ascorbic acid from 0.1 eq. to 100 eq.

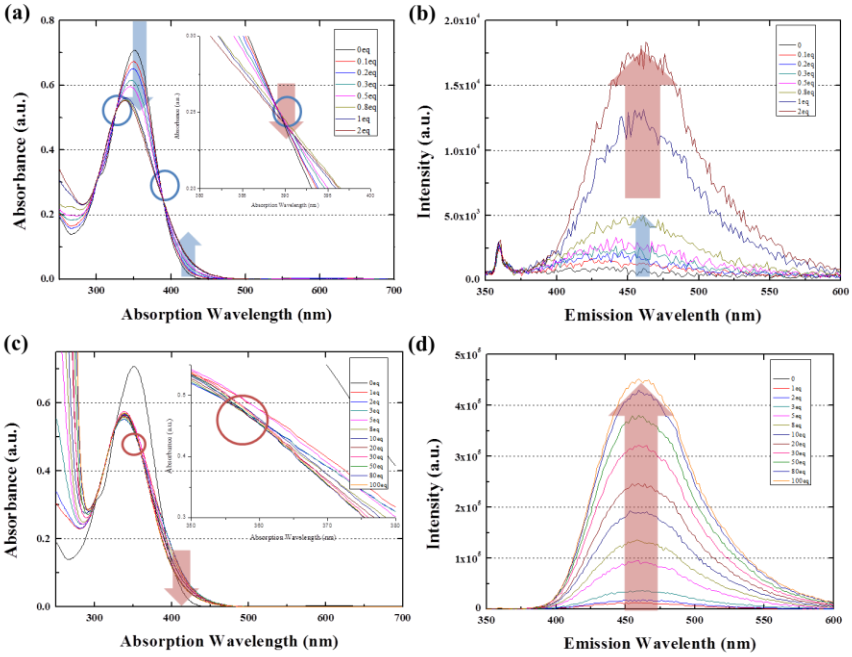

Figure 3.4. Absorption and PL spectrum change of NN-CN-TFFP in MeOH solution (2 x 10^{-5} M) with injection of ascorbic acid in two ranges. one is from 0.1 eq. to 2eq., (a) and (b), respectively. Another is from 1 eq. to 100 eq., (c) and (d), respectively.

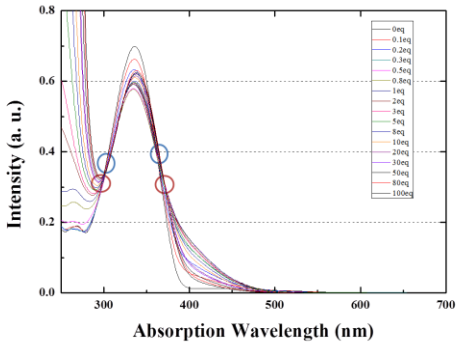

Figure 3.5. Absorption spectrum change of IN-CN-TFFP in MeOH solution (2 x 10^{-5} M) with injection of ascorbic acid from 0.1 eq. to 100 eq.

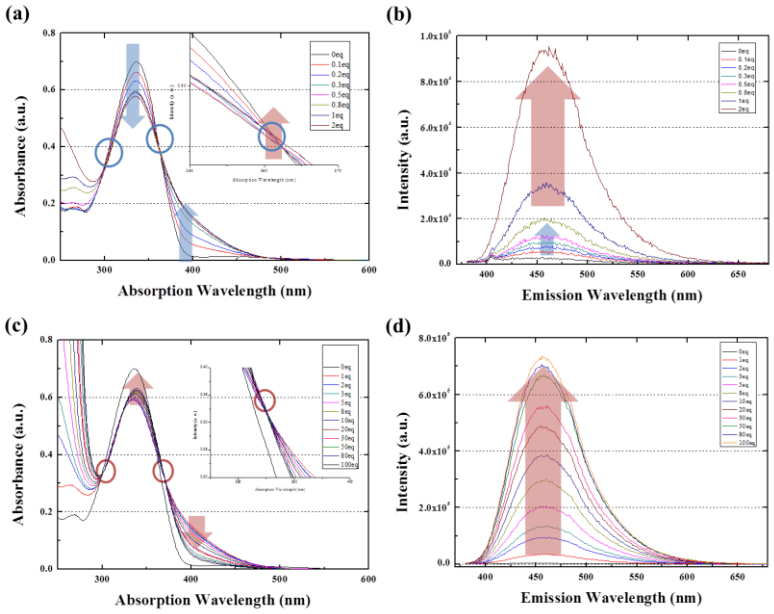

Figure 3.6. Absorption and PL spectrum change of IN-CN-TFFP in MeOH solution (2 x 10^{-5} M) with injection of ascorbic acid in two ranges. one is from 0.1 eq. to 2eq., (a) and (b), respectively. Another is from 1 eq. to 100 eq., (c) and (d), respectively.

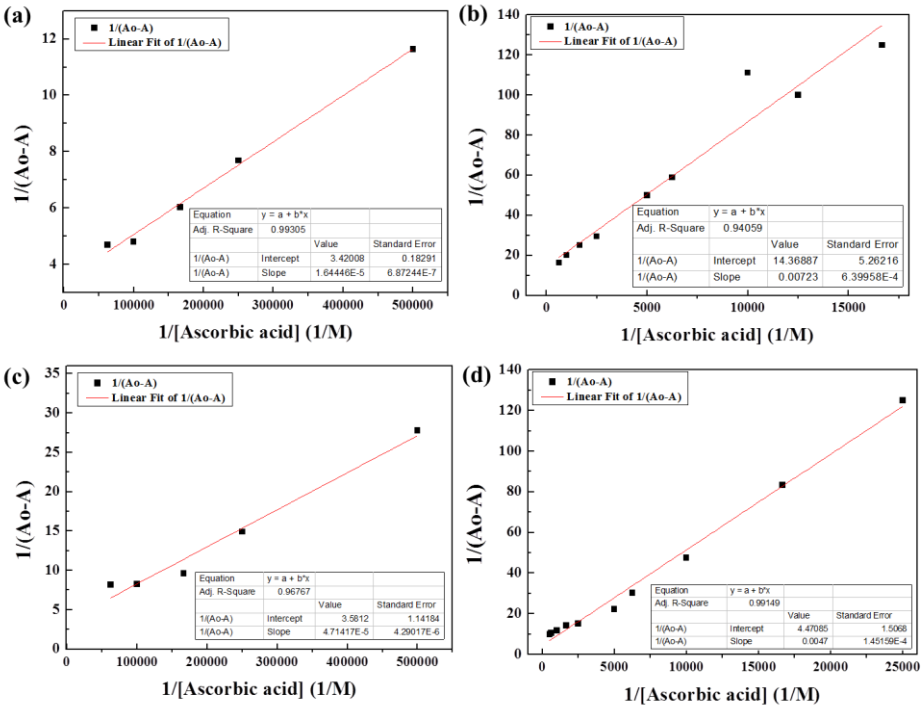

Figure 3.7. Benesi-Hildebrand plot of two different ranges: 2 - 16 x 10^{-6} M ((a), (c)) and 4 - 200 x 10^{-5} M ((b), (d)) of NN-CN-TFFP ((a), (b)) and IN-CN-TFFP ((c), (d)).

3.3.1.2. Selectivity

Selectivity of materials was measured with two different measurements. Ascorbic acid (AA) is sorted as water soluble antioxidant, so water soluble antioxidants were selected like hydroguinone (HQ), L-cysteine (Cys), tyrosol (Tyr), and glutathione (GSH). Also, butylated hydroxyl toluene (BHT) was chosen as the representative of fat-soluble antioxidants which is soluble in methanol. Radical molecules were dissolved in methanol with 2 x 10^{-5} M concentration. The stock solution of analytes in water solution, except BHT in MeOH solution, was prepared and injected to the solution of sensors with 100 equivalent amounts to sensing molecules.

NN-CN-TFFP exhibited good selectivity. Fluorescence was turned-on with high contrast only by ascorbic acid. ESR signals were completely turned-off only by ascorbic acid, but HQ molecules also acted as an antioxidant of NN-CN-TFFP and reduced a half of radicals. However, it has been reported that TEMPO radicals were reduced to hydroxylamine by these water-soluble antioxidants. The selectivity difference between TEMPO[2,3] and nitronyl nitroxide might originate from the reactivity of radicals. Different from a TEMPO radical, nitronyl nitroxide radicals are delocalized through two N-O moieties, so it might be hard to react with other species. Similarly, imino nitroxide having shorter conjugation length than nitronyl nitroxide are expected to have poor selectivity. Not only ascorbic acid, but also GSH and Tyr turned on the fluorescence of the imino nitroxide. Moreover, most of antioxidants switched off the ESR signals of IN-CN-TFFP.

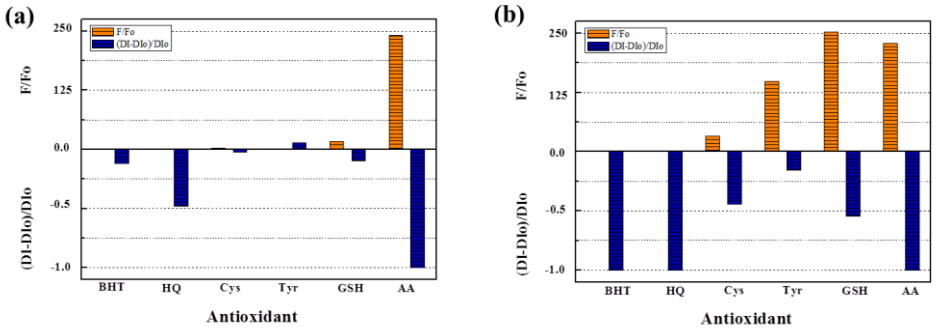

Figure 3.8. ESR (blue bar) and PL (orange bar) selectivity of NN-CN-TFMBE (a) and IN-CN-TFMBE (b) among antioxidants.

3.3.2. Sensor Properties in Solid States

As we discussed in the previous chapter, NN-CN-TFFP and IN-CN-TFFP formed self-assembled nanostructure in aqueous condition. For exploring water compatibility of the AA sensors, nanoparticles of the sensor molecules were prepared. The fabrication method was simple precipitation method discussed in the Chapter 2. Water volume fraction was 70 % to make nanoparticles with about 100 nm size. Total concentration of radical molecules was 2 x 10^{-5} M.

Nanoparticles exhibited dual-mode detection ability like methanol systems. Figure 3.10 depicted the ESR spectra and fluorescence change with various ascorbic acid concentrations. ESR signal turned off with ascorbic acid, while fluorescence turned on. However, the detection range is changed in aggregated states. ESR signals were remained until the addition of AA reached 0.4 mM concentration (Figure 3.9 (a), (c)). Figure 3.9 (b), (d) displayed that fluorescence intensity started to increase from 0.4 mM AA concentration. It linearly increases in the range of 0.4 ~ 2 mM AA concentration. Maximum *F/Fo* of NN-CN-TFFP and IN-CN-TFFP nanoprobes was 15 and 20, respectively. Different sensing behaviors between in the methanol solution and in nanoparticles are presumably attributed to the aggregated states. Paramagnetic nitroxide radicals close to the center of particles should have less chance to react with ascorbic acid even after radicals near surfaces are completely reduced and protonated with AA (Scheme 3.2). Therefore, fluorescence signals started to recover in very high AA concentration where all of radicals in the nanoparticles can be reduced.

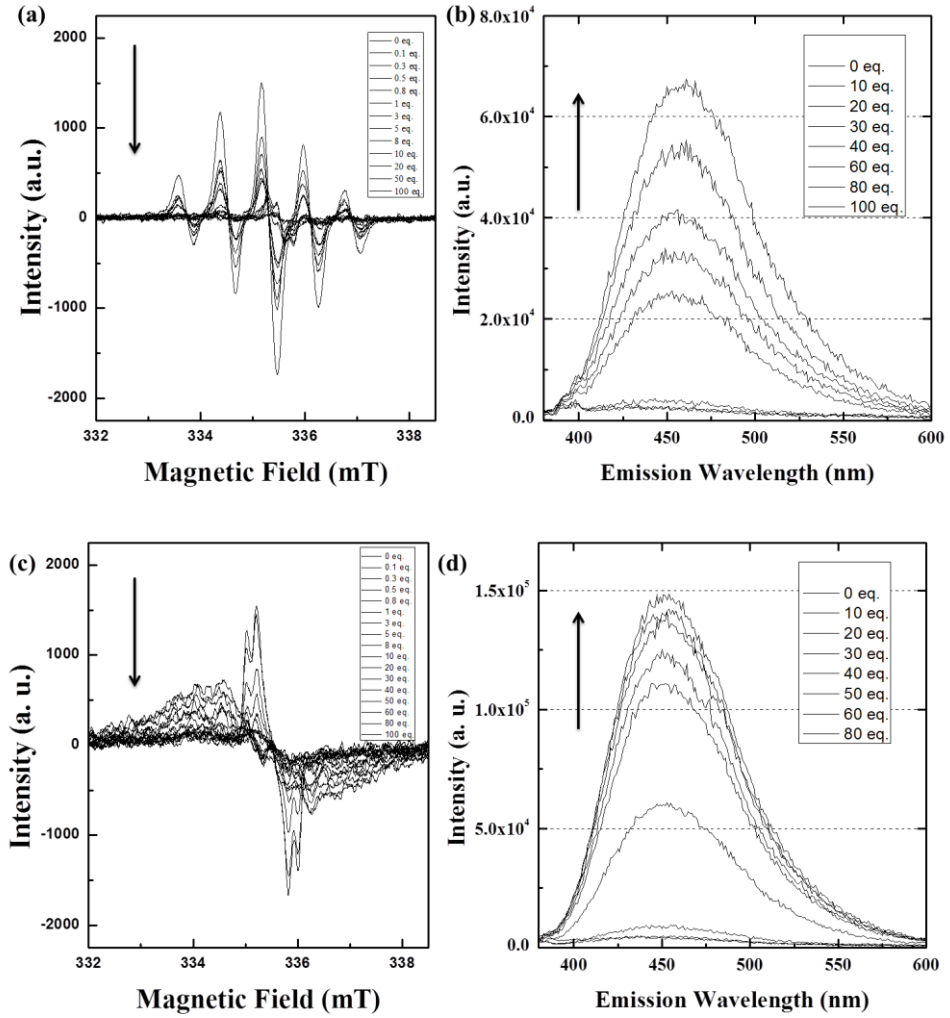

Figure 3.9. ESR (a), (c) and fluorescence (b), (d) spectra of NN-CN-TFFP ((a), (b)) and IN-CN-TFFP ((c), (d)) nanoparticles (0.02 mM in THF/water mixture) in the presence of various AA concentrations (0 – 2 mM).

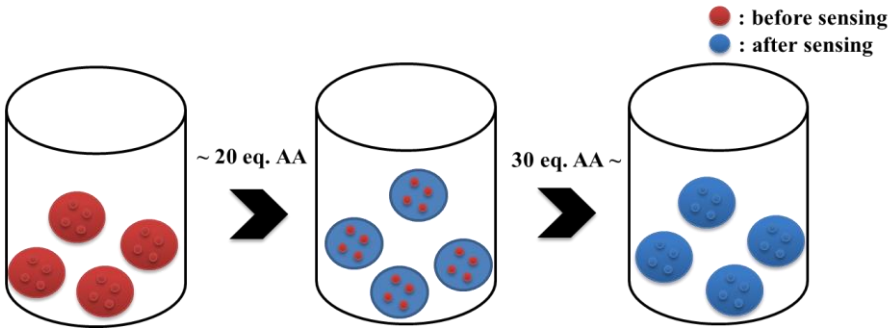

Scheme 3.2. Nanoprobe reaction scheme for the specific ranges.

.

3.3.3. Sensor Properties in Aqueous Systems

3.3.3.1. Fabrication of co-nanoparticles and their fluorescence

Although the advantages of synthesized nitroxide materials, they are still have problems to directly use in biological systems such as a low quantum yield, blue emission colors, and low water compatibility. Therefore, we devised a new strategy to circumvent the problems. The strategy is fabricating co-nanoparticles consisting of the nitroxide molecules as a quencher dopant and water compatible highly fluorescent molecules as nanoparticle frameworks which have similar molecular structures with the dopants. 12EO-CN-TFMBE[9] consists of rigid cyano-stillbene type backbones with two trifluoromethyl groups showing strong intermolecular interactions and hydrophilic poly ethylene glycol moieties for sufficient water compatibility. It has been already reported that 12EO-CN-TFMBE molecules forms highly fluorescent nanoparticles in aqueous systems. (Figure 3.10)

The co-nanoparticles of NN-CN-TFFP and 12EO-CN-TFMBE for aqueous systems were fabricated with the following method. The stock solution of each materials in BHT-free tetrahydrofuran was prepared with 0.5 mg/mL concentration. The solutions of two materials, nanocarriers and sensing molecules were injected into one 20 mL volume glass vial and well-mixed with vortex mixer. The dried solid state materials were obtained after removing tetrahydrofuran by evaporation uder reduced pressure.

Water is poured into the vial, and it was shakened with vortex mixer for 75 seconds. Total concentration of nanocarriers was 0.05 mg/mL for all systems. Two different molecules aggregated together or separately.

Intermolecular interaction between two different molecules is very important to make self-assembled co-nanoparticles. Co-assembly is hard to occur unless the structure of backbone and the sorts of intermolecular interaction are similar. NN-CN-TFFP has three main intermolecular interaction explained in the Chapter 1. These same interactions exsit in 12EO-CN-TFMBE. However, 12EO-CN-MBE does not have trifluoromethyl moiety generating hydrogen bond interaction. Therefore, it is expected that NN-CN-TFFP and 12EO-CN-MBE formed self-assembled nanoparticles separately. This is well explained by the quenching efficiency of these systems. The co-nanoparticle system with NN-CN-TFFP and 12EO-CN-TFMBE shows dramatic photophysical changes with doping concentration increase, while the fluorescence intensity of the system with NN-CN-TFFP and 12EO-CN-MBE does not show significant changes (Figure 3.11).

Co-nanoparticle system consisting of NN-CN-TFFP and 12EO-CN-TFMBE displayed effectively quenched fluorescent signals. Figure 3.11 (a) showed that only 1 wt % dopants makes the fluorescence intensity of nanocarriers a half. The increase of dopants amount reduces fluorescence of nanocarriers gradually. The fluorescence signal with 5 wt % doping concentration is reached to 1/10 of 12EO-CN-TFMBE fluorescence intensity. The intersystem crossing mechanism of quenching were

applicable to this system judging from the energy level. ISC mechanism is operating when SOMO level of radical is located inbetween HOMO and LUMO level of chromophore. The both molecules have good energy matching with 5.16 eV for SOMO of CN-TFFP, 5.89 eV for HOMO of 12EO-CN-TFMBE, and 2.92 eV for LUMO of 12EO-CN-TFMBE (Scheme 3.3). The efficient quenching is explained by the distance between quencher molecule and fluorescent molecule. Electron can be exchanged intermolecularly when two molecules were adjascent each other. Because both molecules exsit in the same particles, most of 12EO-CN-TFFP molecules are right next to NN-CN-TFFP. It is much more efficient system than the solution of quencher and chromophore molecules due to low chance of meeting different molecules.

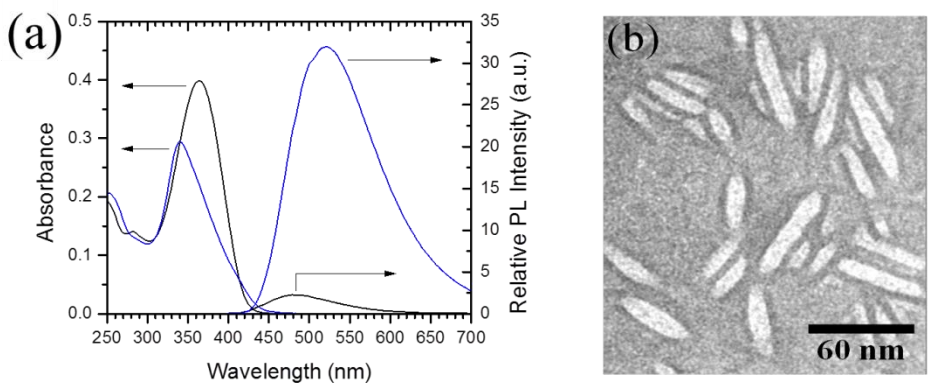

Figure 3.10. (a) Absorption and photoluminescence (PL, excited at 380 nm) spectra of 12EO-CN-TFMBE at 10 μM in THF (black lines) and water (blue lines). (b) TEM image of 12EO-CN-TFMBE self-assembled nanostructures.[10]

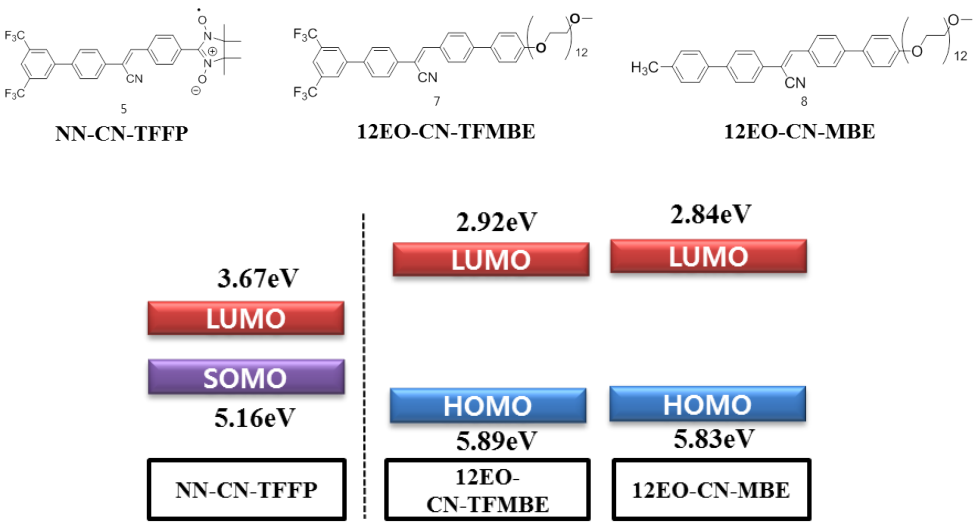

Scheme 3.3. Molecular structure of NN-CN-TFFP, 12EO-CN-TFMBE, and 12EO-CN-MBE and their energy levels measured by cyclic voltammogram.

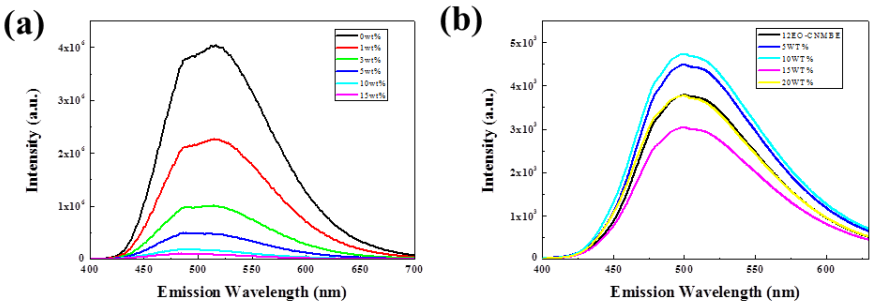

Figure 3.11. PL spectrum change of 12EO-CN-TFMBE (a) and 12EO-CN-MBE (b) by NN-CN-TFFP doping.

3.3.3.2. Properties of Sensors

The optimized doping contcentration was determined with two criterias, contrast and brightness. The fluorescence of co-nanoparticles with various dopant concentrations were recovered by 10 mM ascrobic acid solution in water which is an excessive amounts for complete reaction between probe molecules and analytes. Figure 3.12 (a) described that over 5 wt % dopants makes the on-off ratio more than 4. Together with high on-off ratio, high brightness is desirable for good sensors, since it is hard to distinguish between two dark fluorescent signals even with very high contrast. Although on-off contrast ratio of co-nanoparticles with 5 wt % dopants is the lowest among systems with 5 wt %, 10 wt %, and 15 wt % doping concentrations, it was selected due to relatively high brightness and appropriate contrast.

Fluorescence titration and a stability test were performed with 5 wt % dopants. In the range of less than 1 mM of ascorbic acid solution, fluorescence recovery was linear. The relative fluorescence intensity F_{DQ}/F_Q *versus* the ascorbic acid concentration showed a good linear correlation in Figure 3.12 (b). LOD was found to be 0.06 mM. In the range of more than 1 mM of ascorbic acid solution, the trend of flourescence shows modest increase and come to saturation regime.

The prepared co-nanoparticles have not only water compatibility for applying it in aqueous system, but also longer emission wavelenght and higher quauntum yield than nanoparticles only with NN-CN-TFFP. Maximum emission wavelength of co-

nanoparticles and nanoparticles are 524 nm and 421 nm (Figure 3.13), respectively. Moreover, quantum yield of this system is 3.47 % wheh dequenched by 10 mM ascorbic acid solution, which is two times higher than quantum yield of NN-CN-TFFP nanoparticles, 1.50 %.

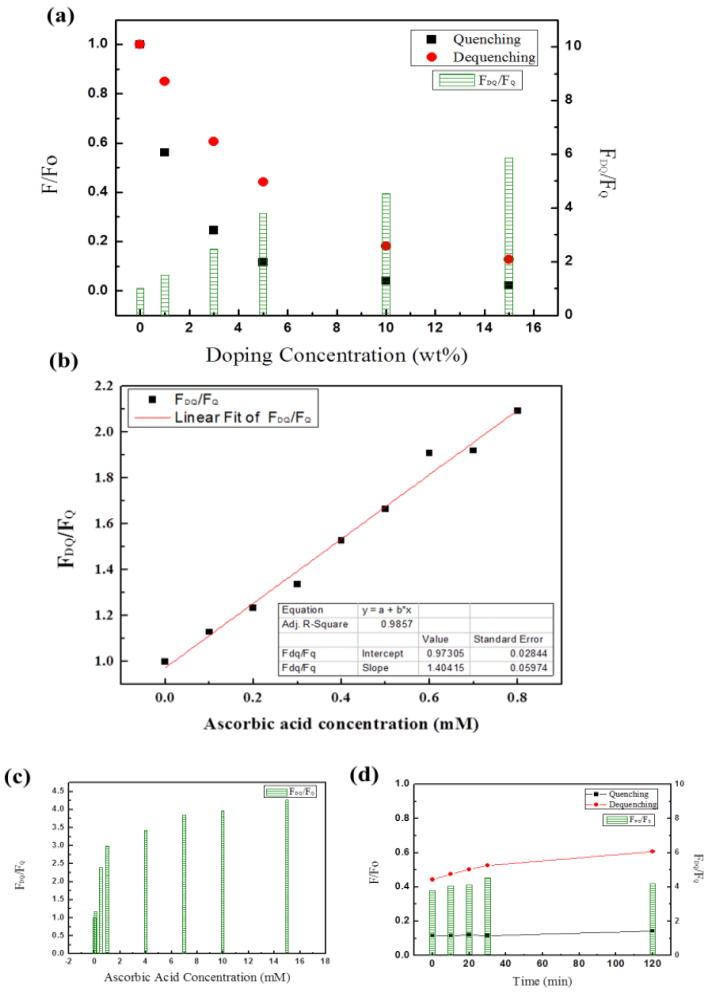

Figure 3.12. (a) PL intensity change in the respect to NN-CN-TFFP doping concentrations and contrast before and after 10 mM ascorbic acid water solution reaction. Ascorbic acid titration (b), (c) and stability of the fluorescence (c) of 5 wt % doped co-nanoparticles.

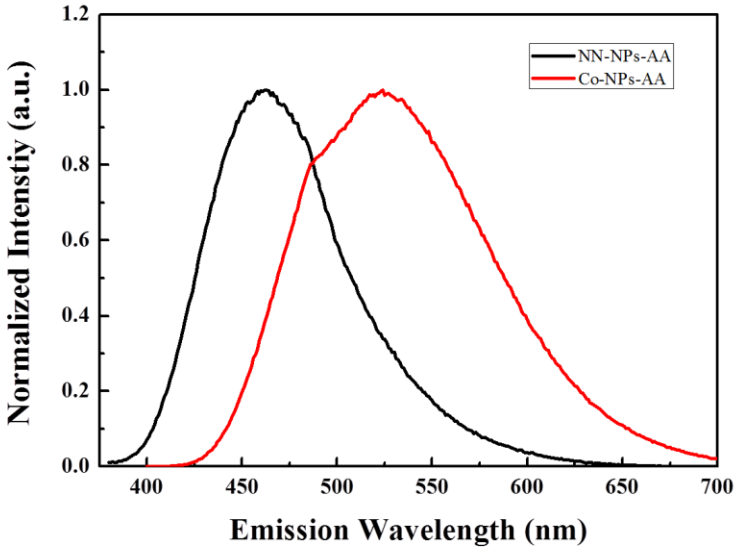

Figure 3.13. Normalized PL spectrum of NN-CN-TFFP nanoparticles (black line) and co-nanoparticles (red line) after excessive ascorbic acid reaction.

3.3.3.3. Demonstration

The photograph in Figure 3.14 (a) demonstrated effeciently quenched 12EO-CN-TFFP nanoparticles by 5 wt % CN-TFFP doping. It shows well-formed nanoparticles with sub-150 nm size confirmed by TEM image. After injection of ascorbic acid solution making total solution as 10 mM, fluorescence signals are turned-on, showing green emission color. Interestingly, TEM images of dequenched particles show bigger size and more dark contrast than quenched nanoparticles (Figure 3.14 (c)). The particles might be swallowed when ascorbic acid getting into the particles for reaction. Then the staining solution might penetrate easily through organic ions or the crack of particles. It has been repoted that ascorbic acid can be penetrated through liposomes covering nanoparticles and react with hydrophobic molecules inside of nanoparticles[2a)]. As we emphasized the dual mode sensing properties of molecules, Figure 3.14 (d) showed that this system was well operated also as an ESR sensor. The peak broadening of ESR signals explained that the distance among NN-CN-TFFP molecules was very close to affect each other

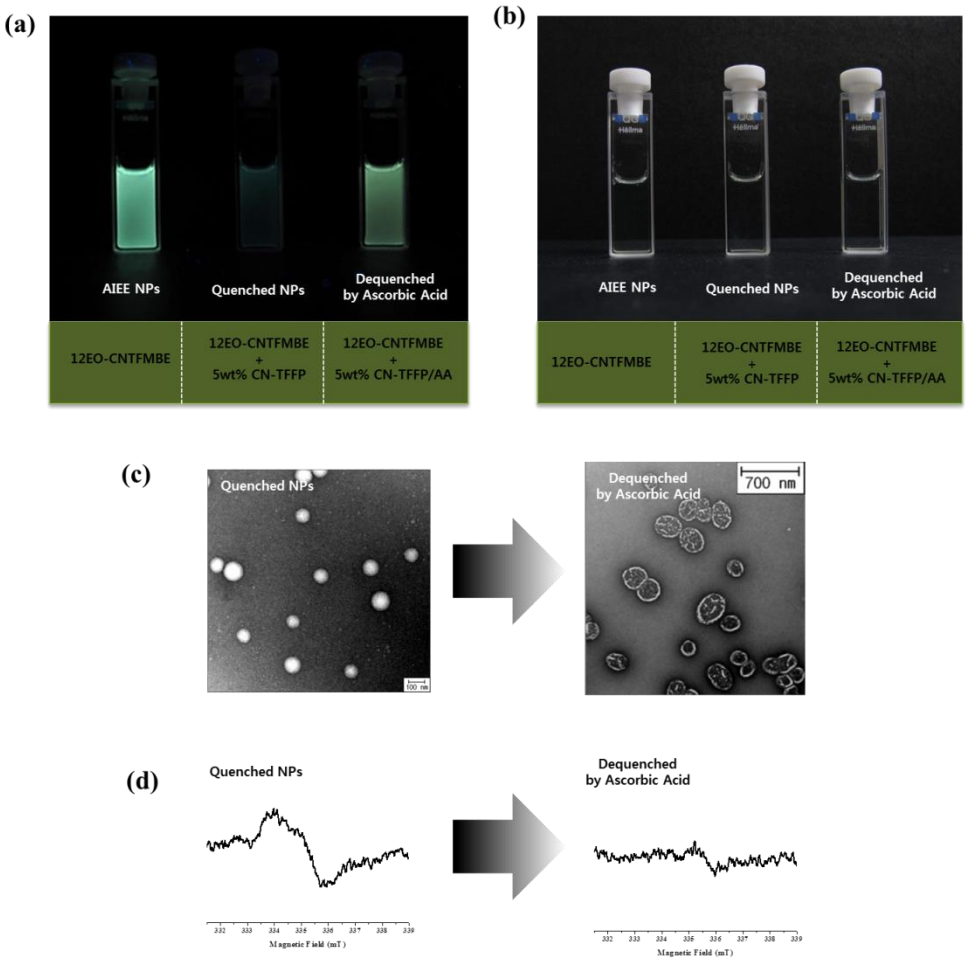

Figure 3.14. Photograph of 12EO-CN-TFMBE, co-nanoparticles, and dequenched co-nanoparticles in aqueous systems under 365 nm UV light (a) and room light (b). TEM images (c) and ESR spectrums (d) were obtained before and after 10 mM ascorbic acid injection.

3.4. Conclusion

NN-CN-TFFP and IN-CN-TFFP we designed were found to interact with ascorbic acid selectively affording huge fluorescence and ESR signal changes. Due to unique π-conjugated backbone consisting of CF_3- units and cyanostilbene, we could utilize them as ascorbic acid sensors in various system such as organic solutions and aqueous suspensions. In organic solution systems, we found that the sensors have good selectivity, high sensitivity, dual-mode detection and a broad detection range. The mechanism underlying the broad detection was suggested through photophysical investigations. Also, their self-assembled nanoparticles bimodally detected ascorbic acid in aqueous suspensions, while having low water compatibility, a low quantum yield, and blue emission colors making hard to apply to biological systems. However, by introducing nanocarriers interacted with the materials to form self-assembled co-nanoparticles, we overcame the weakness of their own materials and showing better properties such as green emission colors, higher water compatibility, and a higher quantum yield. This founding is expected to enhance the possibility of direct detection in biological systems for elucidating biological roles of AA.

3.5. Bibliography

1. a) S. Klebanoff, D. Dziewiatkowski, G. Okinaka, *J. Gen. Physiol.*, **1958**, *42*, 303; b) B.A. Eipper, R.E. Mains, C.C. Glembotski, *Proc. Natl. Acad. Sci.* U.S.A., **1983**, *80,* 5144; c) M.B. Davies, J. Austin, D.A. Partridge, *Vitamin C: Its Chemistry and Biochemistry, The Royal Society of Chemistry*, Cambridge, **1991**.
2. a) K. Ishii, K Kubo, T. Sakurada, K. Komori, Y. Sakai, *Chem. Commun*., **2011**, *47,* 4932 b) D. Pei, J. Hong, F. Lin, Z. Shi, Z. Chen, H. Nie, X. Guo, *Chem. Commun*., **2011,** *47,* 9492
3. W. Chen, X. Wang, X. Tu, D. Pei, Y. Zhao, X. Guo, *Small*, **2008**, *4*(6), 759
4. a) Y. B. Borozdina, V. Kamm, F. Laquai, M. Baumgarten, *J. Mater. Chem*., **2012**, *22,* 13260; b) H. Wang, D. Zhang, X. Guo, L. Zhu, Z. Shuai, D. Zhu, *Chem. Commun.*, **2004**, 670
5. LOD was calculated with the equation using parameters of fitting curves: LOD = 3*(Standard deviation of the curve's intercept)/Slope of the curve)
6. a) G. A. Harirson, *Chemical Methods in Clinical Medicine,* Churchill, London, 3rd edn. **1947**, p.292, b) M. Langlois, D. Duprez, J. Delanghe, M. D Buyzere, D. L. Clement, *Circulation*, **2001**, *103*(14), 1863
7. A. M. Pisoschi, A. F. Danet, S. Kalinowski, J. Aut., *Meth. Man. Chem.,* **2008**, 937651

8. Q. Chen, M. G. Espey, M. C. Krishina, J. B. Mitchell. C. P. Corpe, G. R. Buettner, E. Shacter, M. Levine, *PNAS*, **2005**, *102*(38), 13604
9. C. B. Black, B. Andrioletti, A. C. Try, C. Ruiperez, J. L. Sessler, *J. Am. Chem. Soc*., **1999**, *121*, 10438.
10. S. Shin, S. H. Gihm, C. R. Park, S. Kim, S. Y. Park, *in preparation*

초 록

니트록시드계의 안정한 라디칼을 포함하고 있는 새로운 공액유기분자의 합성, 특성분석, 그리고 응용에 관한 연구

남해림

재료공학부

The Graduate School

Seoul National University

공액유기분자와 연결된 니트록시드 라디칼에 대한 연구는 그 독특한 광학적, 물리적, 전기화학적 특성 때문에 많은 주목을 받아왔다. 물리학, 화학, 생물학 분야의 광범위한 응용 가능성에도 불구하고, 집합체 형태에서의 초분자적 성질들에 대한 불충분한 연구가 응용 가능성을 제한하고 있다. 게다가, 나노구조 형성에 대한

매우 적은 예와 전략들이 보고되었다.

따라서, 우리는 자기조립적 나노구조를 형성하는 라디칼을 포함한 새로운 공액유기분자에 대해 보고하고자 한다. 이 분자는 전략적으로 설계되고 좋은 수율로 성공적으로 합성되었다. 또한 니트록시드 라디칼이 가지는 독특한 특성들이 전자 스핀 공명 분광법과 흡수 분광법, 전기화학적 측정법을 통해 연구되었다. 흥미롭게도, 간단한 재침전법으로 자기조립된 나노입자는 상자성을 띠고 있었다.

더하여, 이 분자는 아스코르빈산 센서로의 응용에서 높은 감응도와 선택성, 넓은 검출 범위, 듀얼 모드 기능과 같은 매우 우수한 성능을 보여주었다. 마지막으로, 우리는 자기조립적 나노구조체를 사용함으로써 수용성 상태에서의 이 분자의 센서 거동을 성공적으로 설명할 수 있었다.

주요어: 자기조립, 나노입자, 니트로닐 니트록시드, 이미노 니트록시드, 형광 센서, 전자 스핀 공명 센서, 상자성, 아스코르빈산

학 번: 2010-20600

List of Presentation

남해림, 권지언, 박수영, **"Novel spin-bearing π-conjugated organogel for exploring spintronic responses"**, 2012 대한화학회 제110회 추계학술발표회, 부산(벡스코), 2012-10-17